

**A Calcium imaging setup at the single ion hit facility at  
GSI and its application to the investigation of Calcium  
response to ion irradiation in mammalian cells**

A dissertation approved by  
the Department of Biology  
Technical University of Darmstadt  
for the degree of Doctor of Philosophy

from

Guanghua Du

born in Henan, China

Referees: Prof. Dr. G. Thiel  
Prof. Dr. M. Löbrich

Date of submission: 11-Dec-2007

Date of examination: 29-Jan-2008

Darmstadt 2008

D17

**A Calcium imaging setup at the single ion hit facility at  
GSI and its application to the investigation of Calcium  
response to ion irradiation in mammalian cells**

dem Fachbereich Biologie der Technischen Universität Darmstadt

zur

Erlangung des akademischen Grades

eines Doctor rerum naturalium

genehmigte

Dissertation von

Guanghua Du

aus Henan, China

Berichterstatter: Prof. Dr. G. Thiel

Mitberichterstater: Prof. Dr. M. Löbrich

Tag der Einreichung: 11-Dec-2007

Tag der mündlichen Prüfung: 29-Jan-2008

Darmstadt 2008

D17

## Declaration

The content of this thesis is based on a published paper A (the appendix of chapter II, a submitted paper B (chapter V) and previously unpublished data and results. I declare that I have performed all the experimental work, data analysis, manuscript preparation presented in this thesis.

I certify that this thesis which I now submit for examination for the award of degree of Doctor of Philosophy, is entirely my own work and has not been taken from the work of others save and to the extent that such work has been cited and acknowledged within the text of my work.

**Paper A.** G. Du, B.E. Fischer, P. Barberet, M. Hei. A fast online hit verification for the single ion hit system at GSI. *Radiat. Prot. Dosim.* **122**(1–4), 320–322 (2006).

**Paper B.** G. Du, B.E. Fischer, K-O. Voss, G. Becker, G. Taucher-Scholz, G. Kraft and G. Thiel. The absence of early Calcium response to high-LET ionizing radiation in mammalian cells. (Submitted to *Radiat. Res.*)

Signature

Date



**A Calcium imaging setup at the single ion hit facility and its application to the investigation of Calcium response to ion irradiation in mammalian cells**

**Content**

<b>1. Introduction.....</b>	<b>1</b>
1.1. Calcium signaling	1
1.2. interaction of Ca <sup>2+</sup> and ionizing radiation	2
1.3. motivation	3
1.4. approach	3
<b>2. The Single Ion Hit Facility at GSI .....</b>	<b>8</b>
2.1. the single ion hit facility	8
2.2. instability	10
2.3. online hit verification	12
<b>3. The Calcium Imaging Setup.....</b>	<b>19</b>
3.1. principle	18
3.2. Calcium imaging setup	19
3.3. fluorescence image	22
3.4. the analysis method	25
<b>4. The Preparatory Experiments.....</b>	<b>32</b>
4.1. Fura-2 loading	31
4.2. photo bleaching and dye leakage	32
4.3. spontaneous Calcium oscillation	34
<b>5. Absence of Ca<sup>2+</sup> Response to Ion Irradiation.....</b>	<b>41</b>
<b>6. Summary / Zusammenfassung.....</b>	<b>59</b>
<b>7. Acknowledgement.....</b>	<b>61</b>



## Chapter I

**Introduction**

Cytosolic free Calcium ions are important second messengers and they play important roles in many signaling cascades regulating numerous cellular functions. Recent studies have shown that the concentration of cytosolic free Calcium ( $[Ca^{2+}]_{cyt}$ ) also regulate the cellular response to ionizing radiation and that radiation with either X-rays,  $\gamma$ -rays and  $\beta$ -rays is able to trigger changes in  $[Ca^{2+}]_{cyt}$ . Up to now, all investigations on the role of  $[Ca^{2+}]_{cyt}$  in radiation responses were done with radiations of low linear energy transfer (LET), namely the aforementioned X-,  $\gamma$ - and  $\beta$ -rays. The response of  $[Ca^{2+}]_{cyt}$  to high LET radiation like heavy ion irradiation has not been investigated before.

**1.1 Calcium Signaling**

The intracellular Calcium in resting cells is mainly sequestered in the endoplasmic reticulum (ER) and the mitochondria. In the ER and in the mitochondria  $Ca^{2+}$  ions are buffered by binding to specific proteins, giving a concentration of free  $Ca^{2+}$  of about 1 mM in the ER. On the other hand, the concentration of free Calcium in the cytoplasm and inside the nucleus ( $[Ca^{2+}]_{intra}$ ) is maintained at a very low concentration of about 10-100 nM. This is more than 3 orders lower than that in the intracellular Calcium stores and in the external medium. Hence the uneven distribution of  $Ca^{2+}$  creates a strong gradient for passive influx into the cytoplasm from both the intracellular  $Ca^{2+}$  stores and the external medium.

Relevant signals, which trigger changes of  $[Ca^{2+}]_{cyt}$ , can accomplish this in two different ways. They can stimulate the opening of Calcium channels in the ER membrane or they can activate  $Ca^{2+}$  channels in the plasma membrane. Because of the gradient an activation of  $Ca^{2+}$  channels results in a sudden increase in  $[Ca^{2+}]_{cyt}$  up to 500-1000 nM [1]. This elevation of  $[Ca^{2+}]_{cyt}$  is monitored by  $Ca^{2+}$  binding proteins and translated into physiological activities. Also because the nuclear envelope pores are permeable to molecules with masses as high as 30-60 kDa the elevation of  $[Ca^{2+}]_{cyt}$  is propagated into the nucleus [2] where it can affect gene regulation and other nuclear processes.

Fig. 1.1 shows a crude overview of the Calcium signaling pathways in mammalian cells. A typical signal transduction cascade involving  $[Ca^{2+}]_{cyt}$  could be as follows: A membrane receptor is activated by a signal. The receptor, which could be a G protein-linked receptor or a tyrosine kinase (RTKs) receptor, then activates Phospholipase C (PLC); PLC in turn hydrolyzes phosphatidylinositol ( $PIP_2$ ) into two second messengers, inositol triphosphate ( $IP_3$ ) and diacylglycerol (DAG).  $IP_3$  binds to a specific  $IP_3$  receptor channel in the membrane of the endoplasmic reticular, which

## I. Introduction

triggers release of  $\text{Ca}^{2+}$  from the ER. In the alternative cascade  $\text{Ca}^{2+}$  enters the cytoplasm directly via Calcium channels.

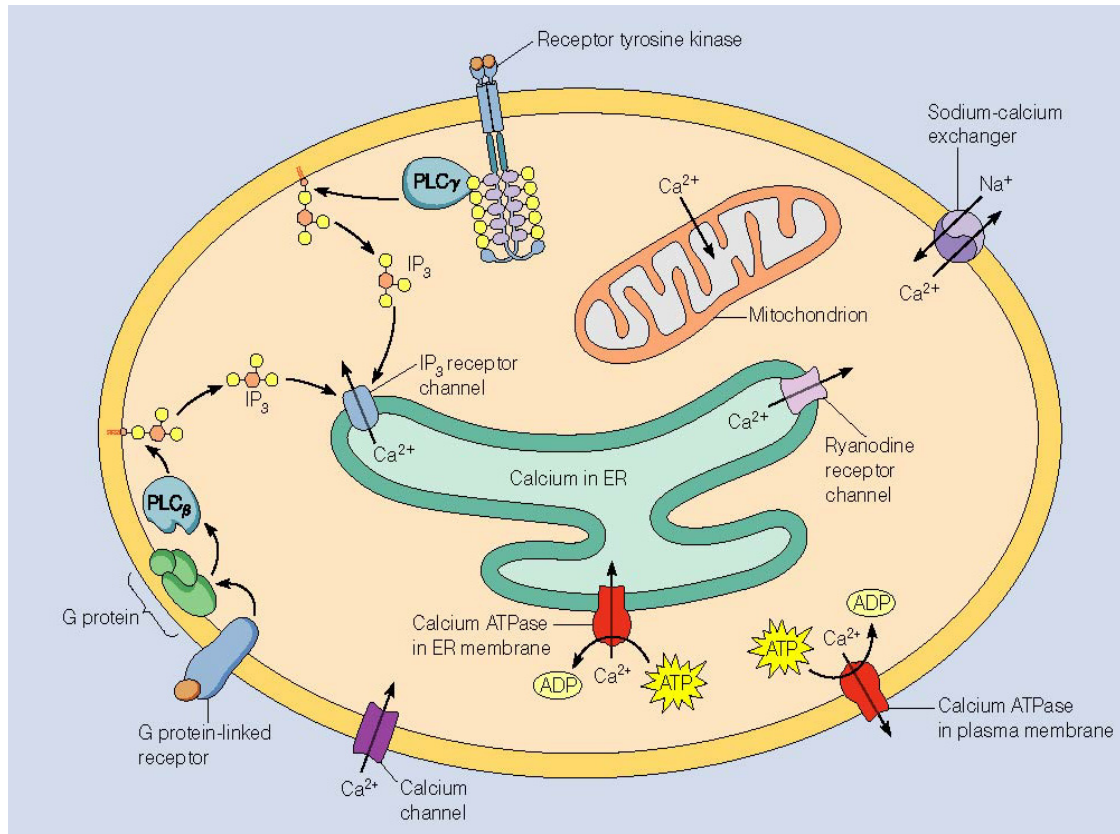


Figure 1.1 Calcium signaling in non-excitable cells. See the introduction for the signaling network in the text above [3].

Upon stimulus induced elevation of  $[\text{Ca}^{2+}]_{\text{cyt}}$  the low resting level is quickly restored. The surplus  $\text{Ca}^{2+}$  is therefore pumped back into the ER or out of the cell via Calcium ATPases under the expense of energy. The energy of the  $\text{Na}^+$  gradient across the plasma membrane is also used to extrude  $\text{Ca}^{2+}$  from the cell ( $\text{Na}^+/\text{Ca}^{2+}$  Exchanger) [1,3].

Free Calcium ions diffuse in the cytosol, bind to proteins and enzymes, change their conformations and activate the targets or modulate their catalytic functions. In its role as a second messenger, Calcium mediates many physiological processes and cell functions. These include cell growth, metabolism, muscle contraction, synaptic transmission, fertilization, secretion and gene expression, etc [1]. On the other hand, extreme alterations in cytosolic  $\text{Ca}^{2+}$  homeostasis can have deleterious effects on cell structure and functions and activate apoptosis [4, 5].

## 1.2 Interaction of $\text{Ca}^{2+}$ and Ionizing Radiation

A number of investigators have indicated that  $[\text{Ca}^{2+}]_{\text{cyt}}$  plays important roles in regulating cellular responses to ionizing radiation. Chelation of Calcium using EGTA/BAPTA-AM reduced or inhibited DNA fragmentation induced by X- or  $\gamma$ -radiation [6-8]. Addition of Calcium in the culture medium partially relieved the  $\gamma$ -ray radiation induced  $\text{G}_2$ -arrest [9]. The elevation of  $\gamma$ -GCS mRNA expression induced by  $\gamma$ -ray radiation was depressed when the cells were treated with different Calcium chelators [10]. Zhao et al have reported that chelation of intracellular Calcium by 5  $\mu\text{M}$  BAPTA-AM suppressed  $\sim 50\%$  of the 5 Gy X-ray induced apoptosis [8].

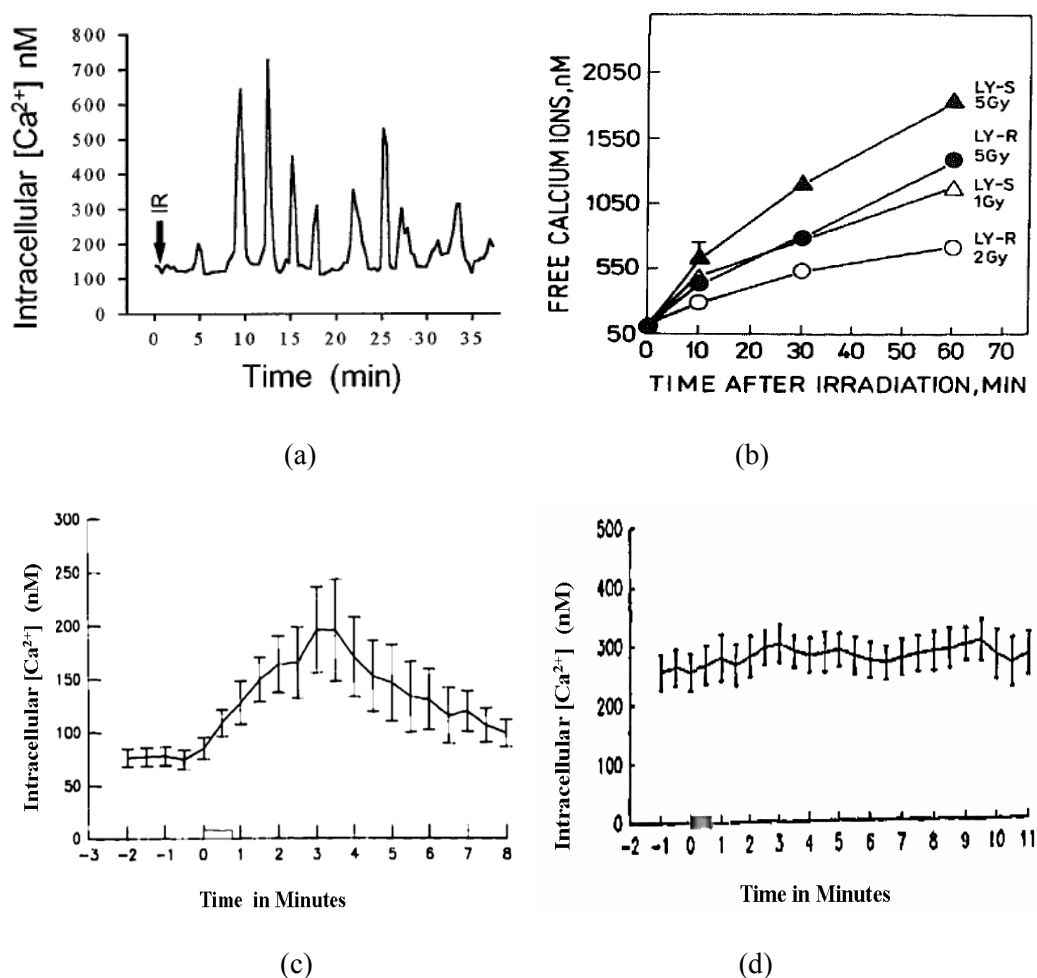


Fig. 1.2 Different response patterns in intracellular Calcium to low LET ionizing radiations. (a) Calcium oscillation in A431 cells irradiated with 1-4 Gy  $\beta$ -ray; (b) continuous Calcium elevation in L5178Y cells irradiated with 1-5 Gy X-ray. LY-R stands for radiation-resistant L5178 cells, LY-S stands for radiation-sensitive L5178 cells; (c) transient Calcium change in MCF-7 cells irradiated with 4 Gy  $\beta$ -ray; (d) no change of  $[\text{Ca}^{2+}]_{\text{cyt}}$  in G1-phase HeLa cells irradiated with 4 Gy  $\beta$ -ray. The data were taken from ref. [11-12, 24].

## I. Introduction

---

Altogether these data show that the cellular response to ionizing radiation is affected by  $[Ca^{2+}]_{cyt}$ . Furthermore, it has also been reported that radiation itself is able to affect  $[Ca^{2+}]_{cyt}$ . Szumiel et al first demonstrated a linear increase of  $[Ca^{2+}]_{cyt}$  between 10 and 60 minutes after X-ray radiation in L5178Y cells [11]. Several groups demonstrated that X-,  $\gamma$ - and  $\beta$ -radiation induced changes of  $[Ca^{2+}]_{cyt}$  in several different cell lines. As shown in Fig. 1.2, these radiation-induced changes of  $[Ca^{2+}]_{cyt}$  occurred in the form of monotonic elevations, oscillations or single transients within minutes after irradiation [7-8,11-13]. However, such responses in  $[Ca^{2+}]_{cyt}$  to radiation have not been observed in all cell lines investigated. Hallahan et al demonstrated that IMR-90, SQ20-B and HL-60 cells showed no apparent response in  $[Ca^{2+}]_{cyt}$  upon  $\beta$ -radiation even with a dose as high as 33 Gy. This lack of response to radiation was found in cells which were still able to elevate  $[Ca^{2+}]_{cyt}$  in response to Bradykinin, a known stimulus for production of  $IP_3$  [14]. A similar absence of calcium signaling after  $\gamma$ -radiation was also reported in vivo [15].

### 1.3 Motivation

It is well known that a prolonged elevation of  $[Ca^{2+}]_{cyt}$  induces cell death by destroying mitochondria and in turn activates apoptotic caspases [16-17]. Since both high  $[Ca^{2+}]_{cyt}$  and ionizing radiation induce cell death, it is interesting to examine the interaction between  $[Ca^{2+}]_{cyt}$  and ionizing radiation. All of the above mentioned results were obtained from low LET ionizing radiations; the cellular Calcium response to high LET ionizing radiation has not been investigated so far.

Ion irradiation is densely ionizing radiation and X-,  $\gamma$ - and  $\beta$ -rays are sparsely ionizing radiation. Ions have an LET of more than 100 keV/ $\mu$ m, which is much higher than the LET of around 0.2-2 keV/ $\mu$ m from X-,  $\gamma$ - and  $\beta$ -radiations. In addition, cells exposed to high LET and low LET radiation have shown differences in many aspects of their cellular response. These include the formation of  $\gamma$ -H2AX foci and the occurrence of the so called oxygen enhancement effect (OER). As shown in Fig. 1.3, X-ray irradiation causes a homogenous formation of foci over the entire nucleus, while ion irradiation causes foci only along the ion tracks in the nucleus.

In addition, Protons and Carbon ions have been successfully used to treat cancer in several countries [18]. In the context of radiotherapy, a response of elevating  $[Ca^{2+}]_{cyt}$  to ion irradiation might enhance the destructive effect of radiation. Therefore, it is worthwhile to investigate the behavior of  $[Ca^{2+}]_{cyt}$  under high LET ionizing radiation.

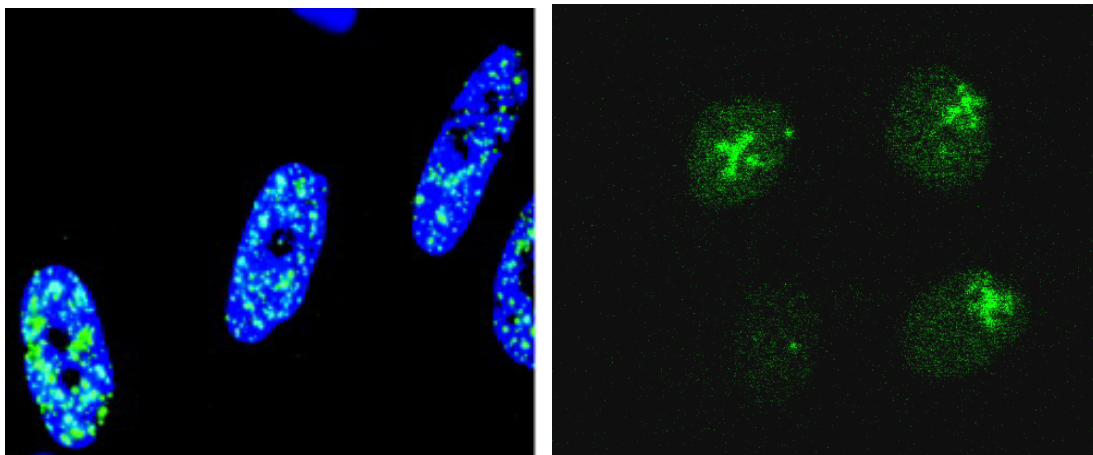


Fig. 1.3 Gamma-H2AX foci formation (green) induced by ionizing radiation. Left: MRC-5 cells, irradiated with 2 Gy of 90kV X-ray (LET~1 keV/ $\mu\text{m}$ ), blue: DNA counter-staining [19]; Right: HeLa cells, targeted-irradiation with 4.8 MeV/n Argon ions of 16 Gy (LET~2000 keV/ $\mu\text{m}$ ). Ions were delivered in a cross pattern: 5 point per axis with 2  $\mu\text{m}$  distance between points, 2 ion hits per point). Note the bottom-left HeLa cell was not irradiated. In the X-ray irradiated cells, the foci were formed homogenously in the cell nucleus, but in the ion irradiated cells, the foci (green cross) were formed only along the ion tracks.

#### 1.4 Approach

The investigation of  $[\text{Ca}^{2+}]_{\text{cyt}}$  signaling in response to ion irradiation was obstructed by several technical problems, which were not relevant in previous experiments with low LET. Firstly, photon or electron radiation results in a homogenous dose distribution in all the irradiated cells, but a cell population irradiated with broad-field ion-beam obtains a random Poisson dose distribution in the cells. The mixture of cells irradiated with undefined numbers of ion hits, even including cells that are not irradiated, introduces a complexity and difficulty to interpret the experimental result. Secondly, most Calcium signals in cells are transient and very sensitive to environmental stress. Ions used to irradiate cells are usually produced by an accelerator. Such an accelerator has usually no facility for providing a physiological environment for the cells under investigation. Also it is not feasible to build a complete instrument for measuring intracellular Calcium at the beamline. This means the Calcium response to ion irradiation is difficult to measure. The un-physiological environment might cause a stress for the cells and disturb its  $\text{Ca}^{2+}$  response to radiation. Also because of the speed of  $\text{Ca}^{2+}$  signals it is not feasible to expose cells to radiation and measure the effect on  $\text{Ca}^{2+}$  signaling later in a specialized laboratory. Relevant transient Calcium response might have disappeared during the transfer of the cells.

The development of a micro beam facility for cell irradiation in the last decade makes it now possible to deliver a well-defined dose to individual cells of interest [20-22]. These microbeam single-ion-hit facilities can irradiate cells precisely at sub-cellular

## I. Introduction

---

regions with a defined and accurate number of ions. Different from the Poisson dose distribution in cells irradiated with a broad-field ion beam, the microbeam facility delivers desired doses to selected cells. At the single ion hit facility in GSI at Darmstadt, cell irradiation has been performed since 2003 [23]. The accelerator UNILAC provides heavy ions from Helium to Uranium for irradiating cells in culture medium at sub-cellular regions with an accuracy of 1.7  $\mu\text{m}$ . In order to investigate the calcium response to heavy ion irradiation, we constructed a ratiometric Calcium imaging setup at the microbeam facility as part of the single ion hit facility. The combination of the two devices allows measuring of intracellular Calcium responses in living cells at high spatial and temporal resolution immediately after defined and local heavy ion irradiation.

### References:

1. D.E. Clapham. Calcium signaling. *Cell* **80**, 259-268 (1995).
2. L. Gerace and B. Burke. Functional organization of the nuclear envelope. *Ann. Rev. Cell Biol.* **4**, 335-374 (1998).
3. W.M. Becker, L.J. Kleinsmith and J. Hardin. *The World of the Cell* (6<sup>th</sup> edition), Pearson Education, Inc./Benjamin Cummings, San Francisco (2005).
4. P. Nicotera, B. Zhivotovsky and S. Orrenius. Nuclear Calcium transport and the role of Calcium in apoptosis. *Cell Calcium* **16**, 279-288 (1994).
5. D.J. McConkey, S.C. Chou, S. Orrenius and M. Jondal. NK cell-induced cytotoxicity is dependent on a  $\text{Ca}^{2+}$  increase in the target. *FASEB J.* **4**, 2661-4 (1990).
6. M.D. Story, L.C. Stephens, S.P. Tomasovic and R.E. Meyn. A role for calcium in regulating apoptosis in rat thymocytes irradiated in vitro. *Int. J. Radiat. Biol.* **61**(2), 243-251 (1992).
7. D.W. Voehringer, M.D. Story, R.G. O'Neil and R.E. Meyn, Modulating  $\text{Ca}^{2+}$  in radiation-induced apoptosis suppresses DNA fragmentation but does not enhance clonogenic survival. *Int. J. Radiat. Biol.* **71**(3), 237-243 (1997).
8. Q. Zhao, T. Kondo, A. Noda and Y. Fujiwara, Mitochondrial and intracellular free-Calcium regulation of radiation-induced apoptosis in human leukemic cells. *Int. J. Radiat. Biol.* **75**(4), 493-504 (1999).
9. Y.C. Du, S. Gu, J. Zhou, T. Wang, H. Cai, M.A. MacInnes, E.M. Bradbury and X. Chen, The dynamic alterations of H2AX complex during DNA repair detected by a proteomic approach reveal the critical roles of  $\text{Ca}^{2+}$ /Calmodulin in the ionizing radiation-induced cell cycle arrest. *Mol. Cell Proteomics* **5**(6), 1033-1044 (2006).
10. K. Teshima, A. Yamamoto, K. Yamaoka, Y. Honda, S. Honda, T. Sasaki and S. Kojima, Involvement of Calcium ion in elevation of mRNA for  $\gamma$ -glutamylcysteine synthetase ( $\gamma$ -GCS) induced by low-dose  $\gamma$ -rays. *Int. J. Radiat. Biol.* **76**(12), 1631-1639 (2000).

11. I. Szumiel, B. Sochanowicz and I. Buraczewska,  $\text{Ca}^{2+}$  mobilization is related to the lethal effect of X-irradiation in L5178Y cells. *Int. J. Radiat. Biol.* **58**(1), 125-131 (1990).
12. R.K. Schmidt-Ullrich, R.B. Mikkelsen, P. Dent, D.G. Todd, K. Valerie, B.D. Kavanagh, J.N. Contessa, W.K. Rorrer and P.B. Chen, Radiation-induced proliferation of the human A431 squamous carcinoma cells is dependent on EGFR tyrosine phosphorylation. *Oncogene* **15**, 1191-1197 (1997).
13. J. Yan, K.K. Khanna and M.F. Lavin, Defective radiation signal transduction in ataxia-telangiectasia cells. *Int. J. Radiat. Biol.* **76**(8), 1025-1035 (2000).
14. D.E. Hallahan, D. Bleakman, S. Virudachalam, D. Lee, D. Grdina, D.W. Kufe and R.R. Weichselbaum, The role of intracellular Calcium in the cellular response to ionizing radiation. *Radiat. Res.* **138**, 392-400 (1994).
15. Takagi K, Yamaguchi K, Sakurai T, Asari T, Hashimoto K, Terakawa S. Secretion of saliva in X-irradiated rat submandibular glands. *Radiat. Res.* **159**(3), 351-360 (2003).
16. D.J. McConkey and S. Orrenius. The role of Calcium in the regulation of apoptosis. *Biochem. Biophys. Res. Commun.* **239**, 357-366 (1997).
17. I. Szumiel. Ionizing radiation-induced cell death. *Int. J. Radiat. Biol.* **66**(4), 329-341 (1994).
18. D. Schulz-Ertner and H. Tsujii, Particle radiation therapy using proton and heavier ion beams. *J. Clin. Oncol.* **25**(8), 953-964 (2007).
19. K. Rothkamm and M. Lobrich. Evidence for a lack of DNA double-strand break repair in human cells exposed to very low x-ray doses. *Proc. Natl. Acad. Sci. USA.* **100**(9), 5057-5062 (2003).
20. M. Folkard, B. Vojnovic, K.M. Prise, et al. A charged-particle microbeam: I. development of an experimental system for targeting cells individually with counted particles. *Int. J. Radiat. Biol.* **72**, 375-385 (1997)
21. G. Randers-Pehrson, C.R. Geard, G. Johnson, C.D. Elliston, D.J. Brenner. The Columbia University Single-Ion Microbeam. *Radiat. Res.* **156**, 210-214 (2001)
22. T. Kamiya, W. Yokota, Y. Kobayashi, et al. Development of an automated single cell irradiation system combined with a high-energy heavy ion microbeam system. *Nucl. Instr. and Meth. B* **181**, 27-31 (2001)
23. M. Heiß, B.E. Fischer, B. Jakob, C. Fournier, G. Becker and G. Taucher-Scholz, Targeted irradiation of mammalian cells using a heavy-ion microprobe. *Radiat. Res.* **165**, 231-239 (2006).
24. D.G. Todd and R.B. Mikkelsen, Ionizing radiation induces a transient increase in cytosolic free  $[\text{Ca}^{2+}]$  in human epithelial tumor cells. *Cancer Res.* **54**, 5224-5230 (1994).

### Chapter II

## The Single Ion Hit Facility

The history of ion microbeam facility dates back to 1953 when Zirkle and Bloom used polished jaws as collimator to obtain an ion beam with a diameter of several micrometers. Their first study was using this microbeam to irradiate parts of individual cells in order to study the cellular response [1]. Later on, many ion microbeams were developed, but most facilities have been devoted to the field of ion beam analysis and material science, but not in radiobiology [2]. Since the beginning of 1990s, some groups became interested in the radiobiological processes which cannot be observed using a broad beam, and several microbeams were developed for cell irradiation at Columbia University (USA), the Gray Cancer Institute (United Kingdom) and JAEA (Japan). These microbeams use modern computers and automation techniques to deliver a defined number of ions into sub-cellular organs in a large amount of cells with a targeting accuracy of several micrometers [3-5]. Different from the Poisson dose distribution in cells irradiated with a broad-field ion beam, the microbeam facility can deliver defined doses (number of ion hits) to irradiated cells, and leave non-targeted cells in the same population un-irradiated. These newly developed microbeams have been used as powerful tools for studying the process of the so called bystander effect, the adaptive response as well as the low dose effect [6-9]. This successful application has attracted more groups to develop microbeams for cell irradiation [10-15].

In this context also the heavy ion microprobe at GSI has been modified to a single ion hit facility for cell irradiation; the first successful experiment was performed in 2003 [13]. Since then, the performance of the facility has been constantly improved; a recent development of this facility is presented in this chapter.

### 2.1 The Single Ion Hit Facility for Radiobiology

The single ion hit facility is part of the microprobe at GSI, which provides ions from Helium to Uranium with energies up to 11.4MeV/nucleon produced by the UNILAC accelerator [16]. As shown in Fig. 2.1, the system works as follows: the accelerated ions enter the object slit of the microprobe and are focused onto the target plane by the magnetic lens (quadru-pole triplets). A beam switch in front of the object slit is used to deflect the beam away from the entrance of the magnets lens in 200 ns. The magnetic beam deflector in front of the lens deflects the focused ions to places in the target plane defined by the coordinate-generator. The focused ions are introduced into air through a vacuum window made of 200 nm thick  $\text{Si}_3\text{N}_4$  coated with 20 nm thick gold and  $50 \mu\text{g}/\text{cm}^2$  CsI. When the ions penetrate the vacuum window, a cloud of secondary electrons is generated from the surface of the window. These secondary electrons are attracted to a Channeltron<sup>TM</sup> detector and amplified to be used as the signal for single ion detection [17].

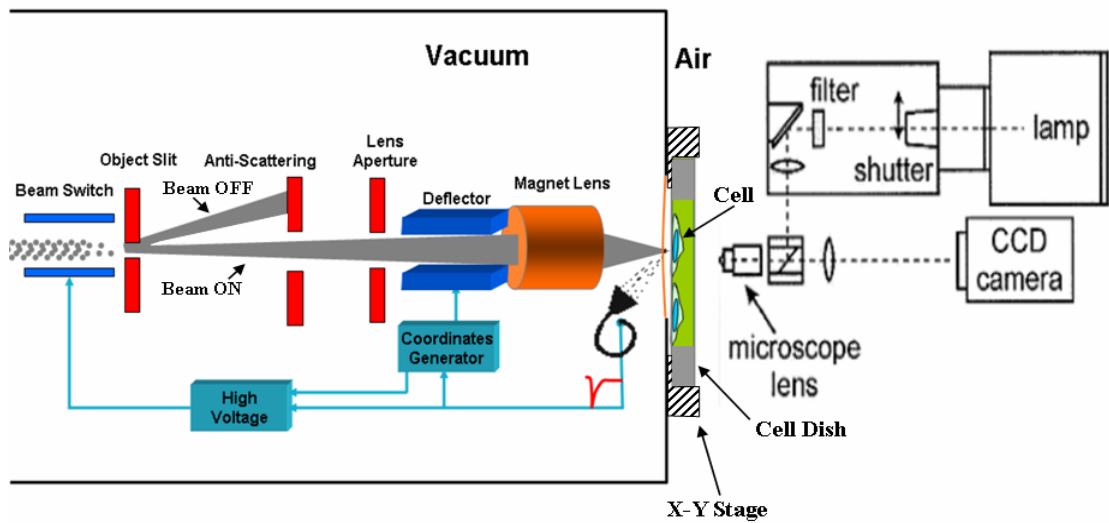


Fig. 2.1 The single ion hit facility for cell irradiation at GSI.

For the irradiation of living cells, the beam has to pass through air and must then be focused on cells in liquid nutrient medium. However, normally ion beams are transported and focused in vacuum. Most of traditional beam focus techniques used in vacuum is not feasible in air except scanning transmission ion microscopy (STIM).

In the facility illustrated in Fig. 2.1, the microbeam is focused onto the plane of the cells by STIM in the following way: The cell dish is removed, a copper micro-grid is placed into the plane of the cells, and an image of the grid is produced by scanning ion transmission microscopy as illustrated in Fig. 2.2.

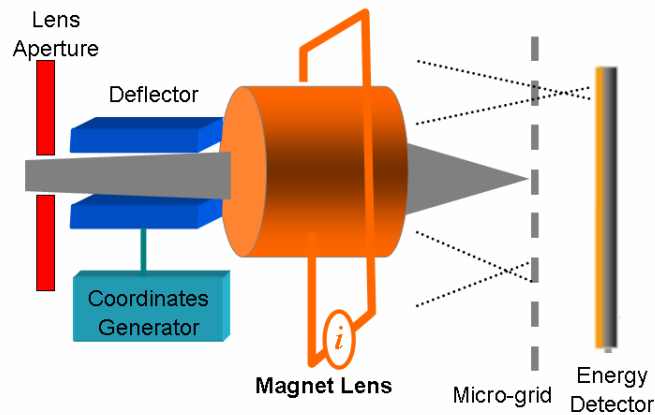


Fig. 2.2 The principle of beam focusing using STIM. The beam focus is tuned by adjusting the focal length of the magnetic lens (by changing the current of the magnetic lens), while the plane of the micro-grid is fixed.

The microbeam is scanned over the copper micro-grid in X and Y, the energy spectrum (E) of the transmitted ions is collected by an energy detector behind the micro-grid and the data (X, Y, E) are stored. When an ion penetrates a grid-bar it loses

## II. Single Ion Hit Facility

---

energy. Therefore, one gets an image of the micro-grid, when one is mapping only events with reduced energy. Like in traditional scanning electron microscopy, one can adjust the focal length of the beam by adjusting the current of the magnet lens. Therefore one can get a sharp image by properly adjusting the lens current until the focal plane of the beam is at the plane of the grid (the plane of the cells).

Normally the beam possesses a rate of  $\sim 200$  ions per second and a beam spot of  $0.7 \mu\text{m}$  diameter in air. Using a scintillator, one can see the beam with a CCD camera and determine the amount of deflection to hit the target. An automated X-Y cell stage is mounted on the flange of the vacuum window and behind the flange is a home-made fluorescence microscope mounted on a movable platform. For a cell irradiation experiment, cells are seeded and grown in a cell dish made of stainless steel with a Polypropylene foil as dish bottom. The cells are normally nucleus-stained using Hoechst 33342 which eases the automatic cell-recognition by the software through fluorescence microscopy. Before the irradiation, the cell dish is closed with cover glass with nutrient buffer inside, and then placed vertically into the x-y stage. The cells in one field of view are recognized automatically by the computer and marked with red crosses at the center of cell nuclei, where the cell should be hit with a defined number of ions. When the irradiation in one field of view is finished, the cell stage moves to the next field of view.

Previous microbeam facilities using collimating technique have a fixed beam, and the cell stage is driven by motors to the beam position for irradiation [3-5]. The advantage of the system at GSI over previous facilities is that the microbeam is moved rapidly with the magnetic deflector to each cell within a field of view, and the X-Y stage is only necessary to move to the next field of view. It is therefore inherently faster than systems using a collimated microbeam. In addition, the focused microbeam has less scattered ions than the collimated microbeam, which gives a well defined LET. Up to now, the activity of this facility is mainly devoted to examine the cellular bystander response to ionizing radiation of high LET [18-19].

### 2.2 Instability

To precisely hit individual cells with an aiming accuracy of a micrometer, not only the beam spot must be very small, but also the positioning of the beam must be very precise. In particular, the position of undeflected microbeam should be known at any time. One also needs to know the position of the cells, and the voltage needed to deflect the microbeam to a particular cell position. To this end, the microbeam (in the form of a light spot on a scintillator) and the cells are observed by the same microscope-camera setup.

Ideally, the position of the undeflected beam is stable and only measured once a day. Then it is only necessary to measure the position of the cells to be irradiated. Unfortunately, the apparent position of the beam drifted over 10 to  $15 \mu\text{m}$  within an hour during the experiment. Happily, it could be proved by scanning transmission ion microscopy that the microbeam-position and the X-Y stage which carries the cell dish

or scintillator was stable within 0.5 to 1  $\mu\text{m}$  for one day. So the microscope-camera setup must have been unstable. The reason for that was that the microscope-objective and the CCD-camera were mounted on a common platform which could move relative to the beam axis due to thermal fluctuations.

To induce the influence of the thermal fluctuation, the cave of the facility was air conditioned and the UV lamp was isolated from the platform. Before an experiment, the facility is heated overnight to reach thermal equilibrium (magnetic lens current and UV lamp are switched on). As shown in Fig. 2.3, the temperature of the platform still varied around 1°C during the day and the platform drifted 2-3 micrometers due to its temperature change. However, the temperature of the platform varied more than 1°C due to disturbance of the thermal equilibrium during the irradiation experiment (e.g. to open and close the cave), thus the drift of the apparent beam was more than 3 micrometers.

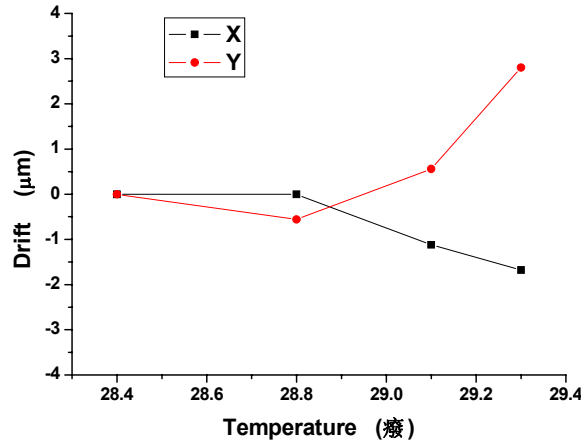


Fig. 2.3 The drift of the platform in X and Y direction in 10 hours during the day.

Another solution was used to reduce the influence of the drift of the platform by mounting the microscope objective rigidly on the small chamber carrying the X-Y stage. As illustrated in Fig. 2.4, if the beam focus, visualized by the scintillator, is initially imaged on position  $\mathbf{P}_0$  on the CCD camera (Fig. 2.4a), it will be imaged on  $\mathbf{P}_1$  on the CCD camera when the platform moves a distance of  $\mathbf{d}$  in the direction of x-axis under the influence of thermal fluctuations (Fig. 2.4 b). If the microscope objective has a magnification of 20 the distance between  $\mathbf{P}_1$  and  $\mathbf{P}_0$  will be  $20 \times \mathbf{d}$ . When the microscope objective is mounted on the small chamber, the same drift of the platform will shift the image of the focus only the distance of  $\mathbf{d}$  on the CCD-camera (Fig. 2.4c). one should note that if the image in the CCD camera drifts a distance of  $\mathbf{d}$ , the translated beam position will be shifted a distance of  $\mathbf{d}/20$ , when the microscope objective has a magnification of 20 times. Therefore, the influence of the thermal drift of the platform on the translated beam position could be much reduced.

## II. Single Ion Hit Facility

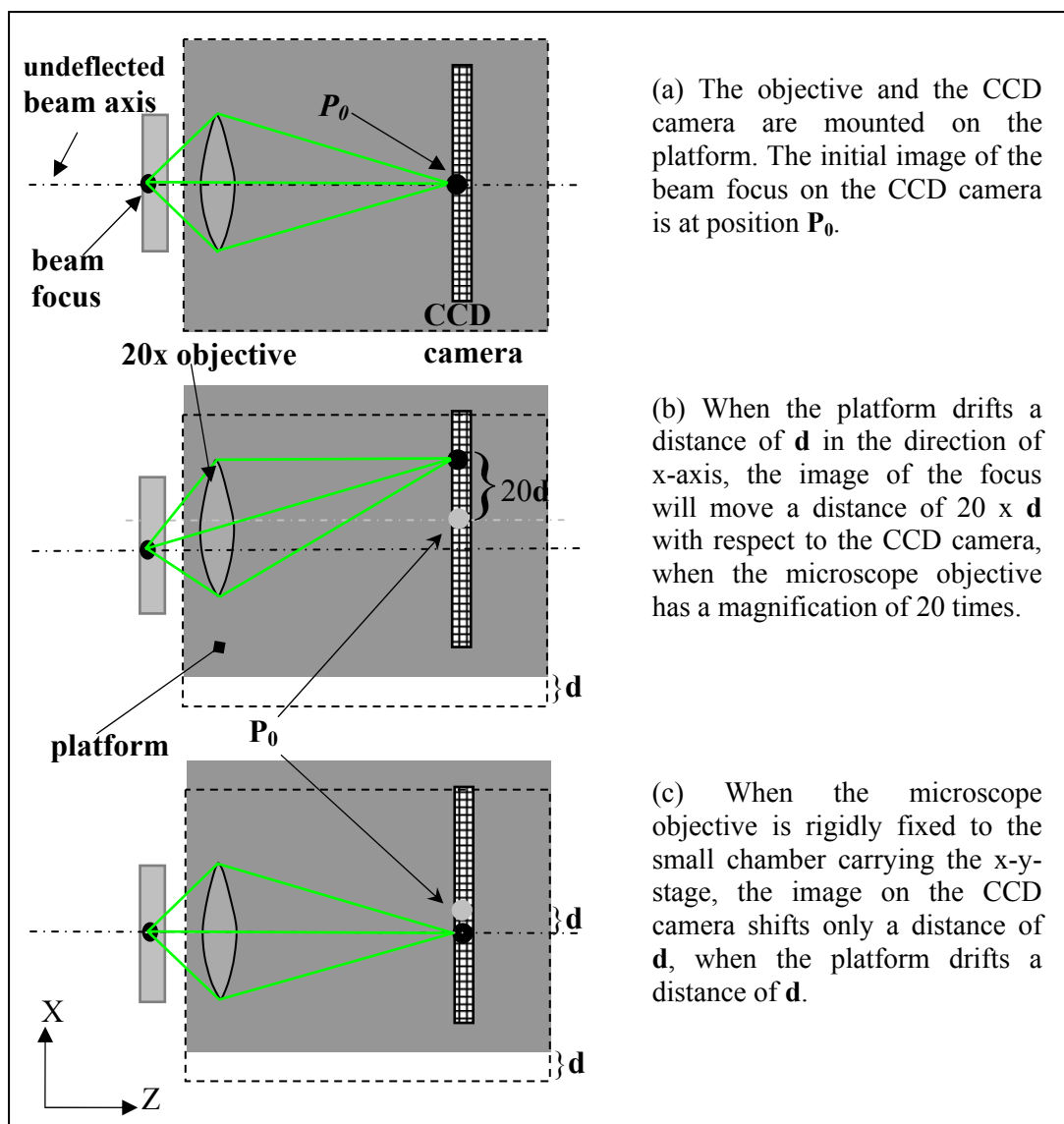


Fig 2.4 The influence of the platform drift on the translation of the beam position.

### 2.3 Online Hit Verification Method

The targeting accuracy of a single ion hit facility is traditionally tested either indirectly by aiming at pre-etched tracks in a nuclear track detector, or directly by making the ion tracks inside cells visible by a stain coupled to special proteins produced in response to ion hits [20]. These methods are time consuming and the targeting accuracy can be verified only after the experiments. To check the targeting accuracy before cell irradiation instead of afterwards, an online hit verification method is developed for the SIHF at GSI. For details please see the appendix at the end of this chapter [21].

## Appendix

# A FAST ONLINE HIT VERIFICATION FOR THE SINGLE ION HIT SYSTEM AT GSI

Guanghua Du\*, Bernd Fischer, Philippe Barberet, Markus Heiss

Gesellschaft für Schwerionenforschung (GSI), Planckstr. 1, 64291 Darmstadt, Germany

## ABSTRACT

For a single ion hit facility built to irradiate specific targets inside biological cells, it is necessary to prove that the ions hit the selected targets reliably as the ion hits usually cannot be seen. That ability is traditionally tested either indirectly by aiming at pre-etched tracks in a nuclear track detector, or directly by making the ion tracks inside cells visible by a stain coupled to special proteins produced in response to ion hits. However, both methods are time consuming and hits can be verified only after the experiment. That means targeting errors in the experiment cannot be corrected during the experiment. Therefore, we developed a fast online hit verification method that measures the targeting accuracy electronically with a spatial resolution of  $\pm 1\mu\text{m}$  before cell irradiation takes place.

## INTRODUCTION

In the last decade, several microbeam irradiation systems have been developed for application in radiobiology. These facilities introduce beams into the atmosphere for hitting living biological targets and can deliver an exact number of particles onto biological targets with an aiming accuracy of micrometers [1-3]. The ability of these tools to discriminate between hit and non-hit cells and to deliver a precise dose is of particular interest to investigate various phenomena related to low dose radiation response [4-5].

A single particle hit facility used for biological applications is based on three main parts: a beam shaping apparatus (collimating and/or focusing) necessary to obtain a micrometric beam size, a precise target positioning system, and a microscope used to localise the cell. To expose specific targets inside biological cells to ions, it is necessary to prove that the ions hit the selected targets reliably as the ion hits usually cannot be seen. That ability is traditionally tested either indirectly by aiming at pre-etched tracks in a nuclear track detector, or directly by making the ion tracks inside cells visible by a stain coupled to special proteins produced in response to ion hits [6]. However, both methods are time consuming and hits can be verified only after the experiment. That means targeting errors in the experiment cannot be corrected during the experiment. Therefore, we developed a fast online hit verification method that

## II. Single Ion Hit Facility

measures the targeting accuracy electronically with a spatial resolution of  $1\mu\text{m}$  before cell irradiation takes place.

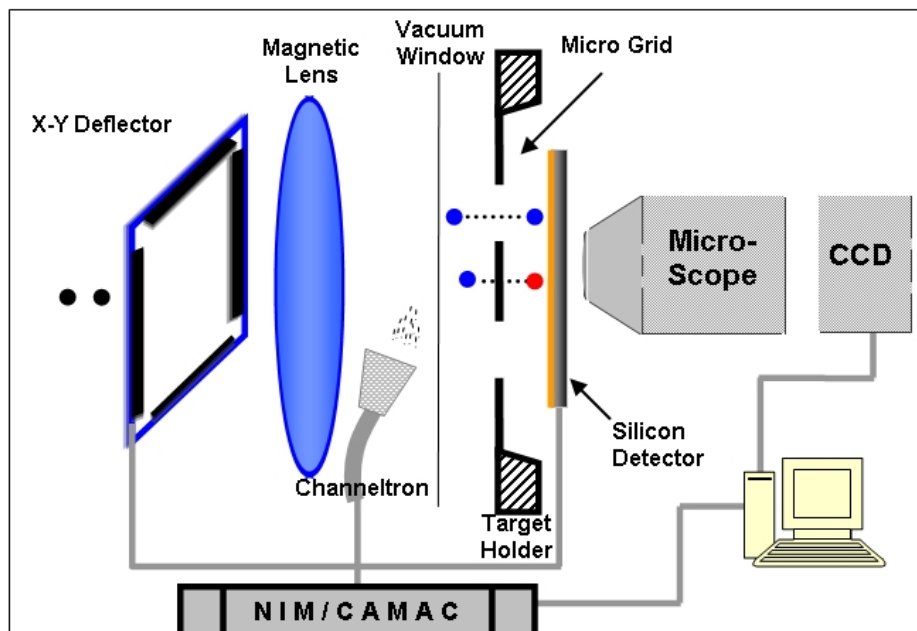


Fig 1. The online hit verification arrangement of the single ion hit system at GSI

### THE ONLINE HIT VERIFICATION METHOD

The Single Ion Hit System for cell irradiation at GSI has recently been adapted to perform targeted cell irradiation. The system is partly shown in Fig.1, more details about this facility are described in reference [7]. To perform the online hit verification, a special micro grid is placed in the plane where the cells are during biological experiments. The grid bars are made of copper and have a bar width of  $6\mu\text{m}$  and a thickness of about  $8\mu\text{m}$  at the middle of the bar. The microscopic image of the grid is shown in Fig. 2. A silicon detector is introduced behind the grid to measure the transmission energy of the delivered ions.

Using the same technique as the one used for irradiating cells, a pre-defined number of ions were delivered only to the grid bars, and the transmission ion microscopy data (ion-hit coordinates and transmission energy) are acquired by a CAMAC acquisition system. The single ions that actually hit the grid should have a lower transmitted energy  $E_1 = E_0 - \Delta E$  due to the energy loss  $\Delta E$  in the bar, and the miss-hit ions that passed through the hole should have an energy close to the initial energy  $E_0$ . Therefore one can check online the global ion-aiming accuracy in the whole targeted window by the distribution of ions of lower transmission energy.

RESULTS AND DISCUSSION

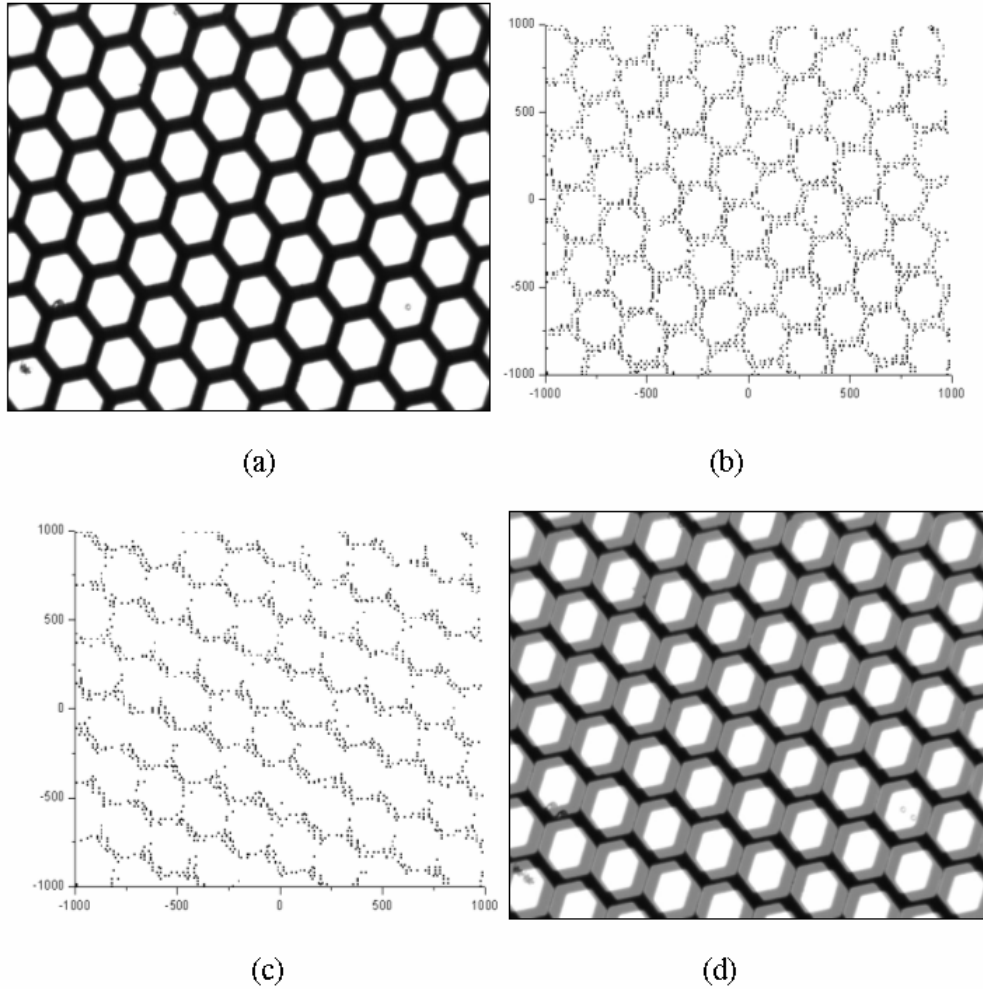


Fig. 2 An online hit verification test at the single ion hit system at GSI. (a) A microscopic image of the micro grid used as a target (bar width:  $6\ \mu\text{m}$ , image size  $360\ \mu\text{m} \times 270\ \mu\text{m}$ ); (b) The hit coordinates derived from the black pixels (the grid bar) in image (a); (c) The coordinates where the ions hit the grid bar; (d) A possible interpretation for the miss-hits (image shift).

Fig. 2 shows an online hit verification test with the single ion hit system at GSI. Only the grid bars shown in the microscopic target image Fig. 2 (a) were chosen to be irradiated by single ions. The irradiation coordinates of ions were derived from Fig. 2 (a) and are shown in Fig. 2 (b). For a perfectly targeting system, ions deflected to any of these coordinates would hit the grid and show some energy loss. As shown in Fig. 2 (c), the coordinate pattern of the lower transmission-energy ions shows that the ions only hit part of the grid. Since the ion position was derived from the microscopic image of the target, this disagreement between Fig. 2 (b) and Fig. 2 (c) indicates some

## II. Single Ion Hit Facility

---

position deviation either in the image-to-beam transformation or in the object-image transformation. According to the beam-calibration technique used at the single ion hit system, this deviation is much larger than the allowable image-to-beam calibration error. It may result from the microscopic image shift due to an imperfect focus (this was repeated after the irradiation). As shown in Fig. 2 (d), such an image shift can cause only the overlapping region similar to Fig. 2 (b) to be hit by the ions.

With this online hit verification method, the global targeting accuracy in a window of  $360\ \mu\text{m} \times 270\ \mu\text{m}$  can be tested with a spatial resolution of  $\pm 2$  pixels ( $\pm 1\ \mu\text{m}$ ,  $\times 20$  lens) at the single ion hit system at GSI.

## ACKNOWLEDGEMENT

This work is supported by the EU under a Marie Curie Research Training Network, Contract No. MRTN-CT-2003-503923.

## REFERENCES

1. M. Folkard, B. Vojnovic, K.M. Prise, et al. A charged-particle microbeam: I. development of an experimental system for targeting cells individually with counted particles. *Int. J. Radiat. Biol.* 72, 375-385 (1997)
2. G. Randers-Pehrson, C.R. Geard, G. Johnson, C.D. Elliston, D.J. Brenner. The Columbia University Single-Ion Microbeam. *Radiat. Res.* 156, 210-214 (2001)
3. T. Kamiya, W. Yokota, Y. Kobayashi, et al. Development of an automated single cell irradiation system combined with a high-energy heavy ion microbeam system. *Nucl. Instr. and Meth. B* 181, 27-31 (2001)
4. M. Folkard, K.M. Prise, B. Vojnovic, et al. The impact of microbeams in radiation biology. *Nucl. Instr. and Meth. B* 181, 426-430 (2001)
5. K.M. Prise, G. Schettino, M. Folkard, K. D. Held. New insights on cell death from radiation exposure. *Lancet Oncol.* 6, 520-528 (2005)
6. B.E. Fischer, M. Heiss, G. Taucher-Scholz, B. Jakob, G. Becker. How to precisely target single living cells with a counted number of ions. GSI Scientific Report (2004)
7. B.E. Fischer, M. Heiss, M. Cholewa. About the art to shoot with single ions. *Nucl. Instr. and Meth. B* 210, 285-291 (2003)

### References

1. R.E. Zirkle, W. Bloom. Irradiation of parts of individual cells. *Science* **117**, 487-493 (1953).
2. G.J.F. Legge. A history of ion microbeams. *Nucl. Instr. and Meth. B* **130**, 9-19 (1997).
3. M. Folkard, B. Vojnovic, K.M. Prise, et al. A charged-particle microbeam: I. development of an experimental system for targeting cells individually with counted particles. *Int. J. Radiat. Biol.* **72**, 375-385 (1997).
4. C.R. Geard, D.J. Brenner, G. Randers-Pehrson and S.A. Marino. Single-particle irradiation of mammalian cells at the radiological Research Accelerator Facility: Induction of chromosomal changes. *Nucl. Instr. and Meth. B* **54**, 411-416 (1991).
5. T. Kamiya, W. Yokota, Y. Kobayashi, et al. Development of an automated single cell irradiation system combined with a high-energy heavy ion microbeam system. *Nucl. Instr. and Meth. B* **181**, 27-31 (2001).
6. M. Folkard, K.M. Prise, B. Vojnovic, et al. The impact of microbeams in radiation biology. *Nucl. Instr. and Meth. B* **181**, 426-430 (2001).
7. K.M. Prise, O.V. Belyakov, M. Folkard and B.D. Michael, Studies of bystander effects in human fibroblasts using a charged particle microbeam. *Int. J. Radiat. Biol.* **74**, 793-798 (1998).
8. L.J. Wu, G. Randers-Pehrson, A. Xu, C.A. Waldren, C.R. Geard, Z. Yu and T.K. Hei, Targeted cytoplasmic irradiation with alpha particles induces mutations in mammalian cells. *Proc. Natl. Acad. Sci. USA* **96**, 4959-4964 (1999).
9. S.G. Sawant, W. Zheng, K.M. Hopkins, G. Randers-Pehrson, H.B. Lieberman and E.J. Hall, The radiation-induced bystander effect for clonogenic survival. *Radiat. Res.* **157**(4), 361-364 (2002).
10. T. Reinert, A. Fiedler, J. Skopek, J. Tanner, J. Vogt and T. Butz. Single ion bombardment of living cells at LIPSION. *Nucl. Instr. and Meth. B* **219-220**, 77-81 (2004).
11. K.D. Greif, H.J. Brede, D. Frankenberg, U. Giesen. The PTB single ion microbeam for irradiation of living cells. *Nucl. Instr. and Meth. B* **217**, 505-512 (2004).
12. P. Barberet, A. Balana, S. Incerti, C. Michelet-Habchi, P. Moretto and T. Pouthier. Development of a focused charged particle microbeam for the irradiation of individual cells. *Rev. Sci. Instrum.* **76**, 015101 (2005).
13. M. Heiß, B.E. Fischer, B. Jakob, C. Fournier, G. Becker and G. Taucher-Scholz, Targeted irradiation of mammalian cells using a heavy-ion microprobe. *Radiat. Res.* **165**, 231-239 (2006).

## II. Single Ion Hit Facility

---

14. B. Hu, J. Wu, W. Han, X. Wang, L. Wu and Z. Yu. Development of a dose-adjustable  $\alpha$ -particle irradiation facility for radiobiological studies. *Nucl. Sci. Tech.* **16**(2), 102-107 (2005).
15. H. Yamaguchi, Y. Sato, H. Imaseki, N. Yasuda, T. Hamano, Y. Furusawa, M. Suzuki, T. Ishikawa, T. Mori, K. Matsumoto, T. Konishi, M. Yukawa, F. Soga. Single-particle irradiation system to cell at National Institute of Radiological Sciences. *Int. Congress Series* **1258**, 281-285 (2003).
16. B.E. Fischer, The heavy-ion microprobe at GSI-used for single ion micromechanics. *Nucl. Instr. and Meth. B* **30**, 284-288 (1988).
17. B.E. Fischer, M. Heiß, M. Cholewa. About the art to shoot with single ions. *Nucl. Instr. and Meth. B* **210**, 285-291 (2003).
18. P. Barberet, C. Fournier, F. Knauf, M. Heiß, B. E. Fischer and G. Taucher-Scholz. Studies on the induction of the cell cycle regulator CDKN1A (p21) in bystander cells using the GSI heavy-ion microbeam. *Radiat. Res.* **166**, 682–684 (2006) [extended abstracts].
19. C. Fournier, D. Becker, M. Winter, P. Barberet, M. Heiss, B. Fischer, J. Topsch and G. Taucher-Scholz, Cell cycle-related bystander responses are not increased with LET after heavy-ion irradiation. *Radiat. Res.* **167**(2), 194-206 (2007).
20. B.E. Fischer, M. Heiss, G. Taucher-Scholz, B. Jakob, G. Becker. How to precisely target single living cells with a counted number of ions. GSI Scientific Report (2004)
21. G. Du, B.E. Fischer, P. Barberet, M. Heiß. A fast online hit verification for the single ion hit system at GSI. *Radiat. Prot. Dosim.* **122**(1–4), 320–322 (2006).

## Chapter III

**The Calcium Imaging Setup**

Calcium signaling is transient and the duration of the  $[Ca^{2+}]_{cyt}$  change responding to certain stimuli varies from milliseconds to minutes [1-2]. To investigate the Calcium response in cells irradiated with heavy ions, it is very important to be sure that the signal of the Calcium response does not disappear before the irradiated cells are examined. However, due to the requirement of radiation protection concerning ion irradiation, it is impossible to reach the irradiated sample, within the first several minutes after the ion irradiation. Therefore, it was not possible to use an equipment like the one used to measure the previous data [2-4]. To examine the cellular response in  $[Ca^{2+}]_{cyt}$  immediately after the irradiation, we built an online Calcium imaging setup at the single ion hit facility at GSI. Using a ratiometric fluorescence-imaging technique, this system allows us to do Calcium imaging before and immediately after the ion irradiation. This Calcium imaging setup makes the online investigation of cellular response to ion irradiation at sub-cellular regions applicable for the first time at an ion microprobe.

**3.1 Principle**

Although the biological importance of Calcium was found by Ringer more than 100 years ago [5], the first reliable measurements of  $[Ca^{2+}]_{cyt}$  were not performed until the 1960s by Ridgway and Ashley by injecting the photoprotein aequorin into the giant muscle fiber of the barnacle [6]. In 1985 Tsien and his colleagues produced a fluorescent calcium indicator named Fura-2 [7]. Because of its high quantum efficiency and ratiometric property upon binding to calcium ions, it has been widely used for investigating  $[Ca^{2+}]_{cyt}$  in intact cells [8]. Fura-2 possesses an emission spectrum from 450 to 600 nm (maximum~510 nm). As shown in Fig 3.1, the dye has two excitation maxima (the excitation wavelength at which the maximum emission is obtained), one is at 380 nm from the free form Fura-2 and the other is at 340 nm from the calcium-bound Fura-2. The fluorescence emission at 380 nm excitation (F380) decreases, while it increases at 340 nm excitation (F340) with a rising Calcium ion concentration. As shown in Fig. 3.1, the fluorescence monitored at the two excitations (F340/F380) is sensitive in the range of 30 nM to 1.35  $\mu$ M  $Ca^{2+}$  in the medium. The absolute Calcium ion concentration can be calculated with the following equation:

$$[Ca^{2+}] = K_d \left( \frac{R - R_{min}}{R_{max} - R} \right) \left( \frac{S_{f2}}{S_{b2}} \right) \quad (3.1)$$

$$\Delta[Ca^{2+}] \propto \left( \frac{R - R_{min}}{R_{max} - R} \right) \quad (3.2)$$

### III. Calcium Imaging System

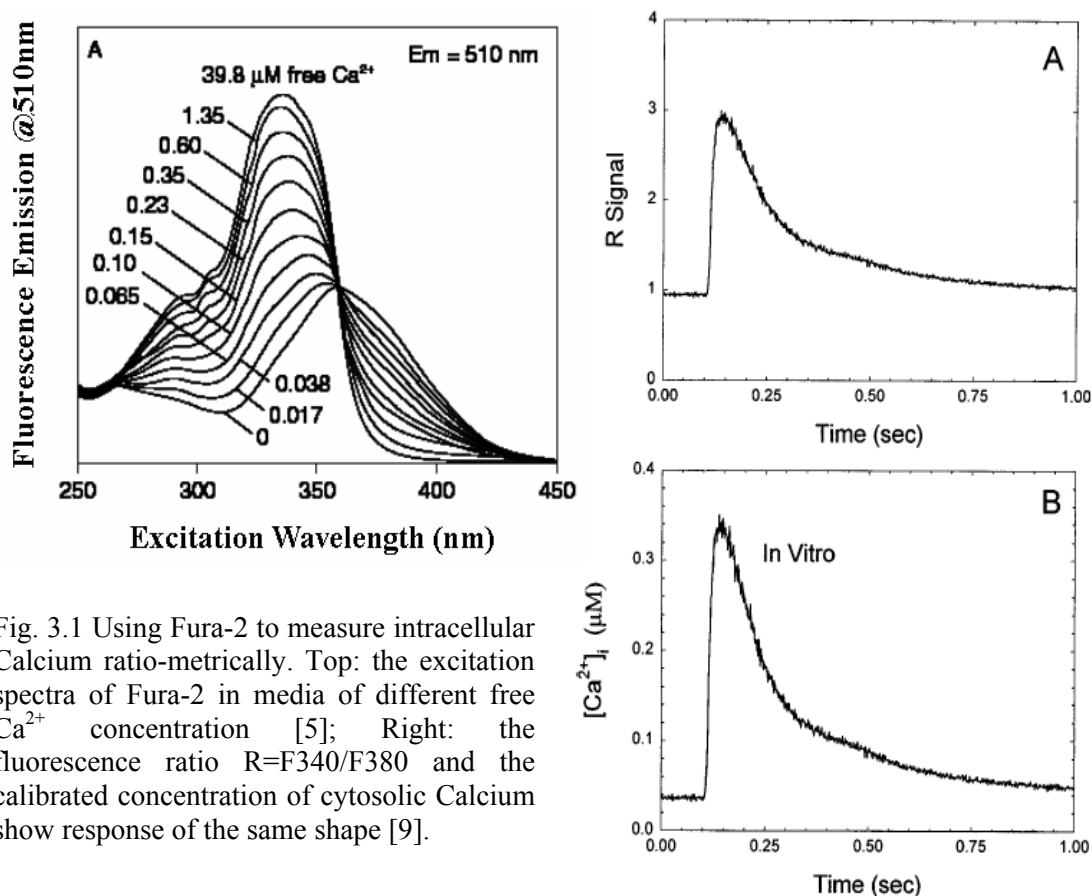


Fig. 3.1 Using Fura-2 to measure intracellular Calcium ratio-metrically. Top: the excitation spectra of Fura-2 in media of different free  $\text{Ca}^{2+}$  concentration [5]; Right: the fluorescence ratio  $R = F_{340}/F_{380}$  and the calibrated concentration of cytosolic Calcium show response of the same shape [9].

Where  $K_d$  is the effective dissociation constant,  $S_{f2}/S_{b2}$  is ratio of the fluorescence emitted from per unit calcium-free and calcium-bound Fura-2 molecules excited at 380 nm,  $R$  is the fluorescence ratio  $F_{340}/F_{380}$ ,  $R_{min}$  and  $R_{max}$  represent the ratio at zero  $[\text{Ca}^{2+}]_{cyt}$  and at saturating  $[\text{Ca}^{2+}]_{cyt}$  respectively. Because  $K_d$  and  $S_{f2}/S_{b2}$  are constant at different levels of  $[\text{Ca}^{2+}]_{cyt}$ , the equation can be written as (3.2). As shown in Fig. 3.1 (right), the calibrated  $[\text{Ca}^{2+}]_{cyt}$  has a similar response shape to stimulus as the observed fluorescence ratio  $R$ .

### 3.2 The Calcium Imaging Setup

Based on the ratio-metric fluorescence properties of Fura-2, a ratio-imaging setup was built at the single ion hit facility to measure the  $[\text{Ca}^{2+}]_{cyt}$  in living cells after ion irradiation. The arrangement of the system is illustrated in Fig 3.2.

The Calcium imaging system is placed behind the X-Y stage holding the cell dish. It is composed of a UV lamp (50 W, DC, short arc mercury lamp, HBO50 W/3, Osram Com, Germany), a filter wheel with two excitation filters (a 380 nm filter, cat. 380FS10-12.5 from LOT-Oriel, EU; and a 340 nm filter, cat. FF01-340/26 from Semrock, USA), an emission filter (525 nm filter, cat. HQ525/50 from Chroma Technology Corp., USA), a dichroic splitter (FT 395, Carl Zeiss AG, Germany), a 20x

### III. Calcium Imaging System

objective (Plan Fluor, ELWD, 20x/0.45, Nikon Com., Japan), CCD camera (Pixelfly, PCO AG, Germany), optic elements, peripheral electronics and computer control. To minimize the UV exposure and photo bleaching, we attenuated the excitation light to the lowest intensity required with a neutral density filter (attenuator); a light shutter in the UV light path was only opened during fluorescence imaging. In addition, an aperture restricts the excitation light only to the field of view.

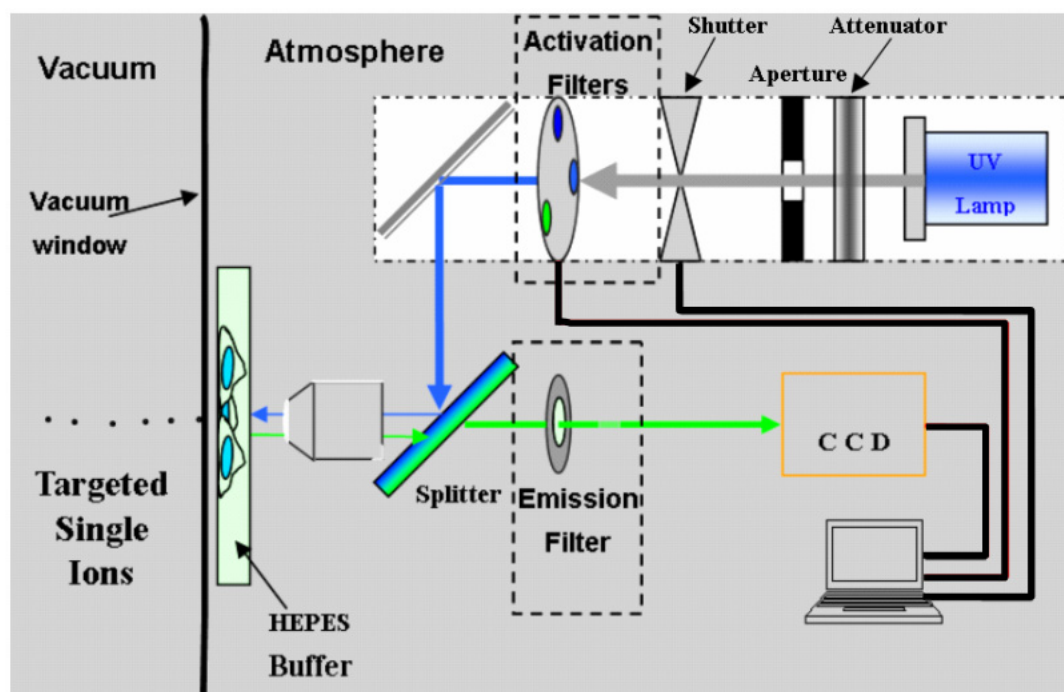


Fig 3.2 The arrangement of the ratio-imaging setup at the single ion hit facility.

Different from an inverted microscope system, the imaging setup monitors the fluorescent light through the medium. It occurred that the fluorescence image had a very bright background when excited at 340 nm UV, but not at 380 nm UV. When the vacuum window was removed, the bright background was much suppressed. The reason for this artifact was that both the bandpass filter for 340 nm light and the emission filter can transmit infra-red light. The vacuum window behind the cell dish is coated with gold reflected the transmitted infrared light into the camera. Therefore an infra-red blocker was also included in the light path in order to block the infra-red light from the UV lamp. As shown in Fig 3.3, the quality of the fluorescence image is much improved when an infrared blocker is used. Otherwise, the background from infra-red light would have corrupted the fluorescence imaging with cells stained with Fura-2.

### III. Calcium Imaging System

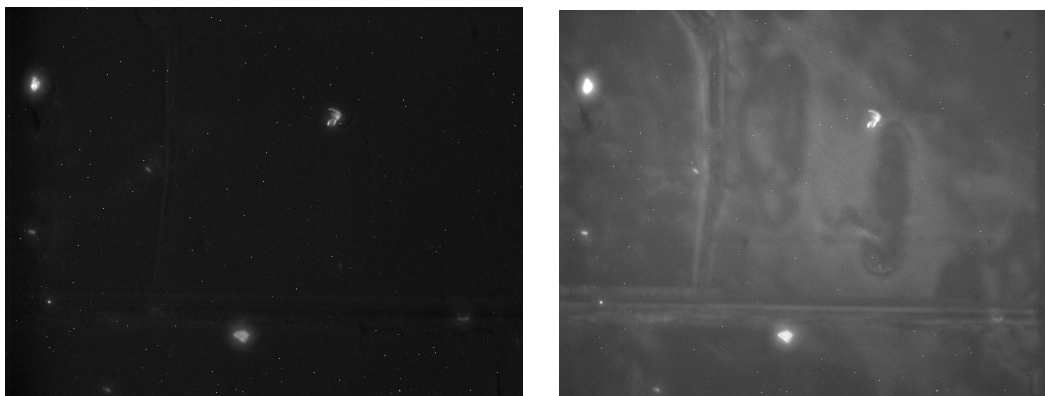


Fig 3.3 Fluorescence images taken at 340 nm UV with (left) and without (right) blocking of infra-red light.

To automate the ratio-imaging, a program was developed in C<sup>++</sup> based on the software development kit of ImagePro Plus 4.0 (an image processing software from Media Cybernetics Inc., USA). Fig. 3.4 shows the control panel of the software module. The software controls the change of filters and opens/closes the shutter via the digital I/Os of a PCI-6713 card (National Instruments, USA). A typical timing of the ratio imaging is illustrated in Fig. 3.5. The system acquires the fluorescence images excited at 340 nm and 380 nm with an exposure time of 200 or 400 ms per image and a frequency of 2-10 image pairs per minute. A ratio image is obtained by the division of the fluorescence image at 340 nm over the fluorescence image at 380 nm.

This code module is integrated into the well established software platform of the single ion hit facility for cell irradiation [10], so that it allows to combine calcium measurements together with cell irradiation. The total recording time, the interval between each pair of snaps, and the time when the targeted irradiation is performed are user-defined. A typical experiment protocol is shown in Fig 3.5: 1) First the targets (red-cross marked cells) are selected manually; 2) then the program starts a three-minute long basal ratio-imaging; 3) after that the program

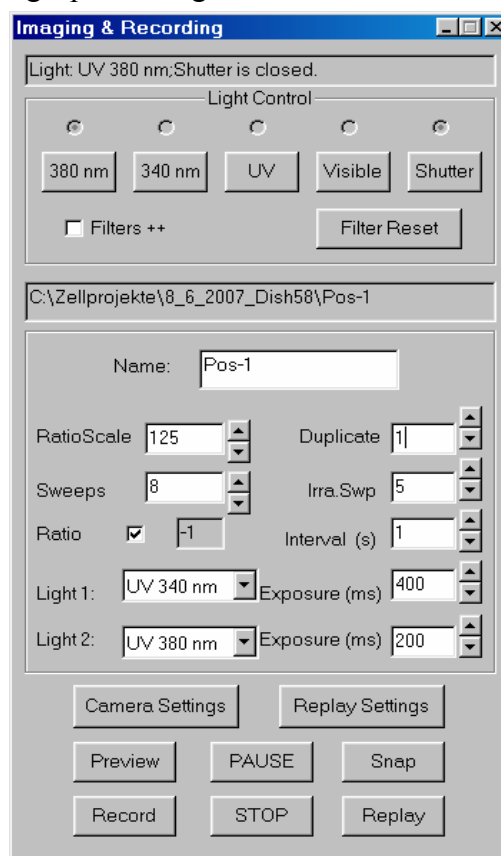


Fig. 3.4 Control panel of the ratio-imaging software.

### III. Calcium Imaging System

switches to the irradiation mode to irradiate the nucleus or cytoplasm of selected cells with a defined number of ions. Depending on the total ion hits delivered in the field of view, the irradiation took several seconds to tens of seconds; 4) immediately after the irradiation, the program resumes the ratio-imaging mode and continues for another 30 minutes. The obtained images are subsequently analyzed cell by cell offline.

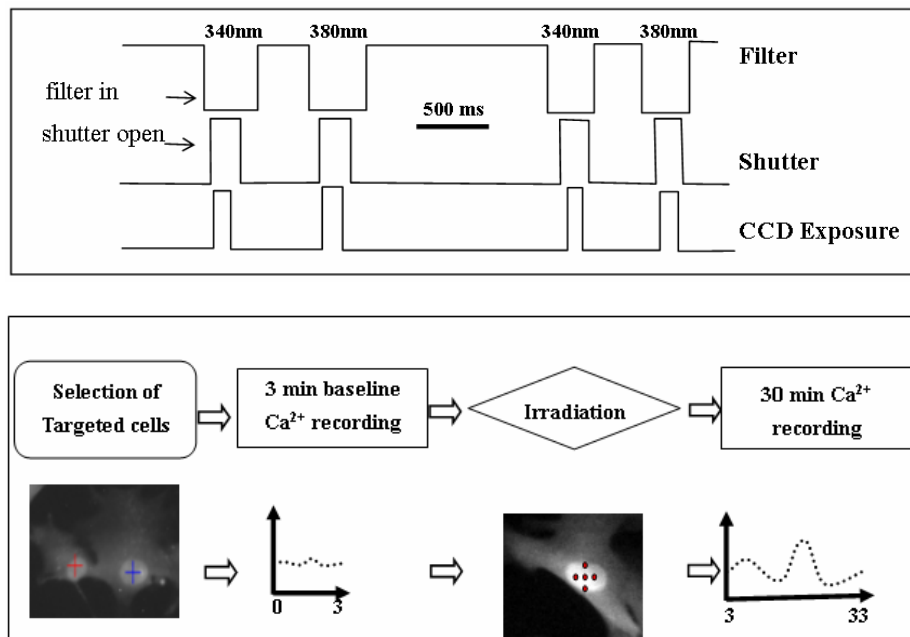


Fig 3.5 Typical timing of ratio-image recording (two pairs) (top) and a typical protocol for calcium imaging measurement together with ion irradiation (bottom).

## 3.3 Fluorescence Image

### 3.3.1 fluorescence background

With the fluorescence imaging system illustrated in Fig. 3.2, the emitted fluorescence collected by the CCD camera comes from the emission from intracellular Fura-2 plus a number of background sources such as: a) the fluorescence from the buffer medium; b) the fluorescence from the foil onto which the cells attach; c) the fluorescence from the vacuum window; d) cellular autofluorescence. It has been reported that the reduced form of nicotinamide adenine dinucleotide (NADH), which is the product of the electron transport chain in all mammalian cells, has an emission at 450-600 nm when excited with UV light [11]. As shown in Fig. 3.6, this auto-fluorescence can be also detected in our Calcium imaging system. It was also reported that phenol red, which is usually used as pH indicator in the culture medium, gives also fluorescence emission that can be detected in this system [12]. However, our experiments using both phenol red-containing and phenol red-free medium showed the same level of fluorescence emission from the medium (data not shown). In addition to the artificial

### III. Calcium Imaging System

---

background, the electronic noise of the CCD camera adds also to the fluorescence signal.

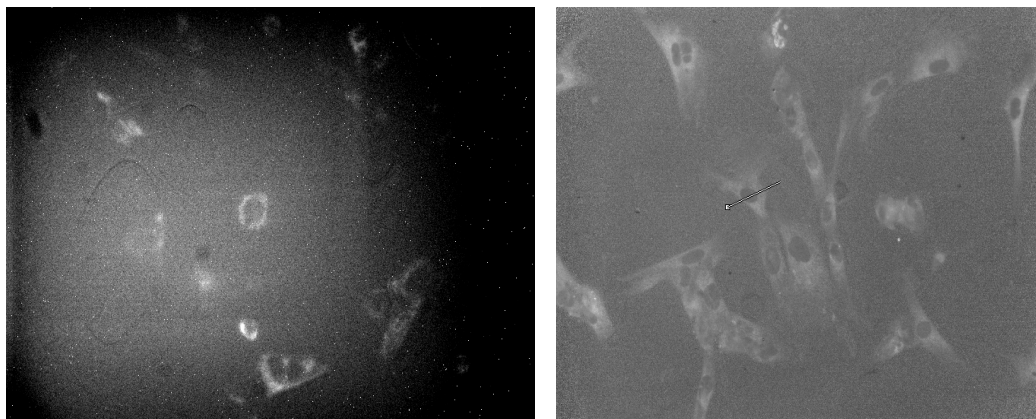


Fig 3.6 Left: the NADH fluorescence in fibroblast cells excited with 340 nm UV (best fit); Right: the ratio image (F340/F380) of Fura-2 stained AG1522-D cells.

As shown in Table 3.1, the fluorescence from different sources was calculated using the pixel intensity in the image. Except the emission from Fura-2 loaded into the cells, most of the fluorescence contribution comes from the culture medium. In total, the measured Fura-2 fluorescence exceeds the background fluorescence by a factor of around 1.2~1.5.

Table 3.1 Different sources that contribute to the fluorescence.

Sources	intensity at 380nm excitation (arbitrary units)	intensity at 340nm excitation (arbitrary units)
Fura-2 in AG1522-D cells <sup>1</sup>	611	570
Medium-AG1522D	360	309
Fura-2 in HeLa cells <sup>1</sup>	268	272
Medium-HeLa	187	181
Polypropylene foil + vacuum window	12	27
NADH <sup>2</sup> (max.) in AG1522-D cells	45	26
CCD noise <sup>3</sup>	18	18

<sup>1</sup> The cells were loaded with 2.5 $\mu$ M Fura-2/AM for 45 minutes at 37°C followed by 30

minutes de-esterification at room temperature.

<sup>2</sup> The autofluorescence mainly took place in the perinuclear region (Fig. 3.6).

<sup>3</sup> The CCD noise is the intensity of an exposure without excitation light.

#### 3.3.2 unevenness of illumination

The use of a CCD camera to collect the fluorescence image has the advantage of obtaining spatial information from many cells in a large field of view at the same time. However, as shown in Fig. 3.7(left), the typical fluorescence image of an area without cell shows an uneven UV illumination all over the field of view (0.57 mm x 0.42 mm). The histogram of the diagonal in the field of view reveals that the fluorescence intensity varies by 300% across the field of view at both excitations.

This histogram also shows a different intensity profile between the F340 and F380 images. As shown in Fig. 3.7-right, the ratio of the fluorescence at both excitations along the diagonal varies over a range of 30%, i.e. the ratio of illumination intensity at 340 nm and 380 nm excitations is inhomogeneous distributed in the field of view. This inhomogeneity would be problematic for comparative analysis of two cells at different places in the field of view, because it results in two unequal nominal  $[Ca^{2+}]_{cyt}$  that is indicated by the ratio F340/F380, even though the two cells have the same level of  $[Ca^{2+}]_{cyt}$ .

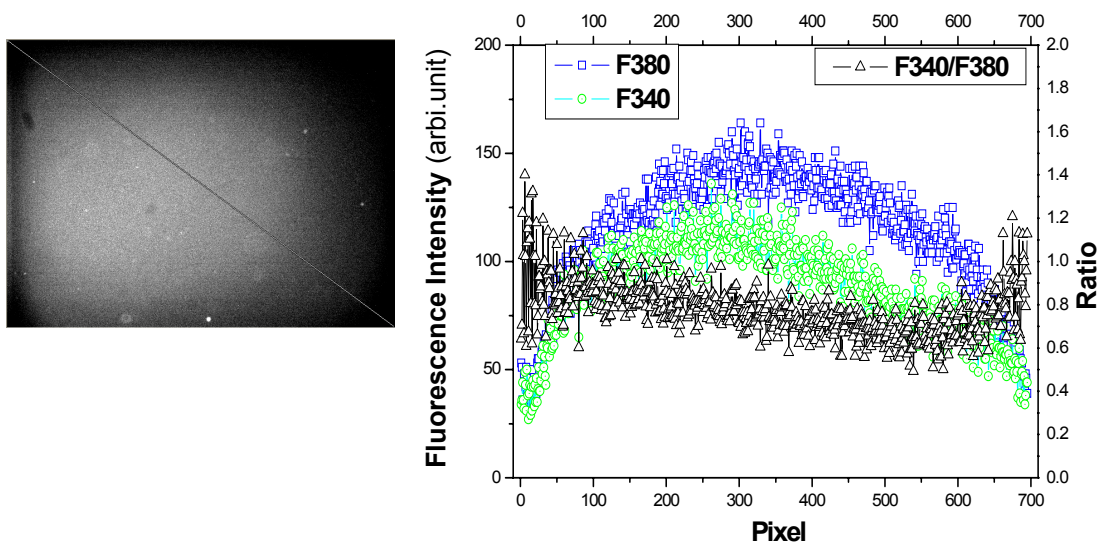


Fig 3.7 The UV illumination is inhomogeneous in the field of view. Left: a typical fluorescence image in an area without cells; Right: the histograms of the fluorescence intensity and the ratio along the diagonal in the left image.

#### 3.3.3 fluctuation of illumination

In preliminary experiments, it was found that the fluorescence intensity of an area without cells is fluctuating in time as shown in Fig. 3.8. Further analysis revealed that this resulted from the instability of the UV illumination. Generally, the illumination at

### III. Calcium Imaging System

340 nm possesses a similar variation as that at 380 nm, the ratio  $F_{340}/F_{380}$  is only slightly influenced by the fluctuation (the relative  $F_{340}$  and  $F_{380}$  varies around 15%, but the mean ratio keeps stable). In some cases, the fluorescence ratio shows sudden changes at the rising or falling edge of the fluctuation as outlined by the green circles in Fig. 3.8. This is because the exposure to 340 nm light is taken 500ms after the exposure to 380 nm light, and the illumination changed between both exposures. These sudden jumps add an error of about 5% to the ratio measurement.

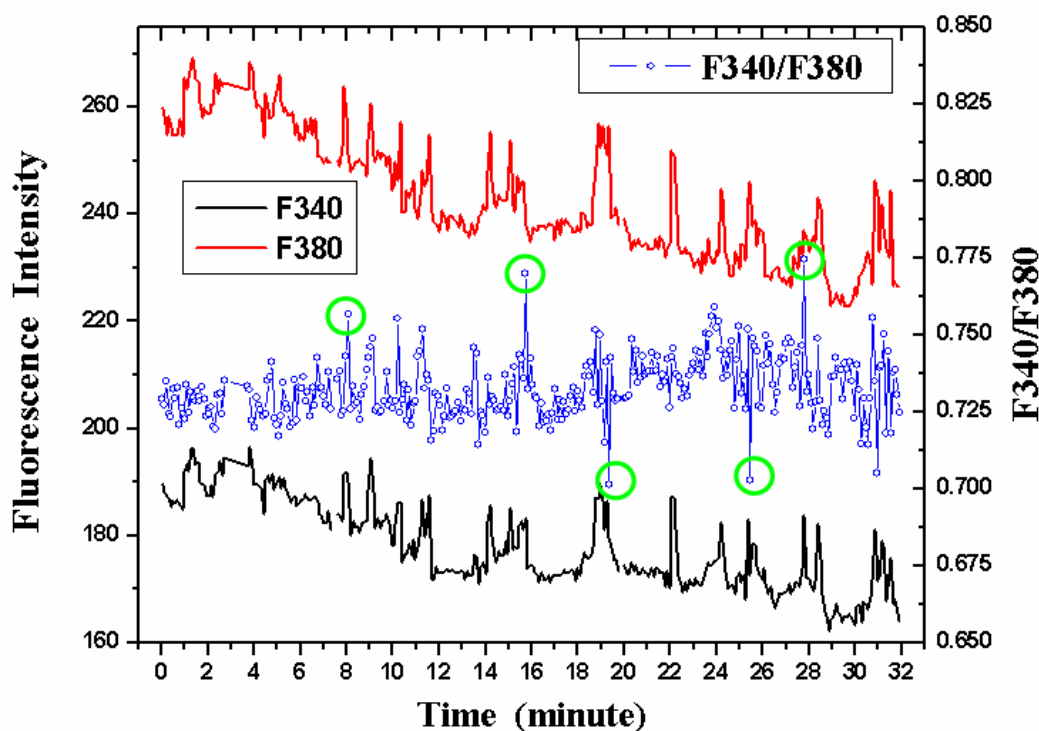


Fig. 3.8 The illumination fluctuation of the UV lamp at 340 nm and 380 nm and its influence on the calculated ratio  $F_{340}/F_{380}$ .

### 3.4 The Analysis Method

The raw fluorescence microscopic images cannot be used to directly obtain the Calcium level inside the cell, because the illumination is inevitably fluctuating in time, and the fluorescence images contain also fluorescence background, and the UV illumination has a locally-uneven and wavelength-dependent intensity profile.

#### 3.4.1 the method

To remove the influence of the illumination fluctuation on the fluorescence imaging, one can compensate the fluctuation in all fluorescence images of a series (e.g. the image series shown in Fig. 3.9a) as if they had been taken at constant illumination. To this end, one first should know the fluctuation level of every image in the series, and

then compensate these raw fluorescence images to an equal level. For this purpose, the method uses an image (Fig. 3.9b) which is taken during the experiment with the same exposure parameters at a field of view without cells. Then the compensation is performed as follows:

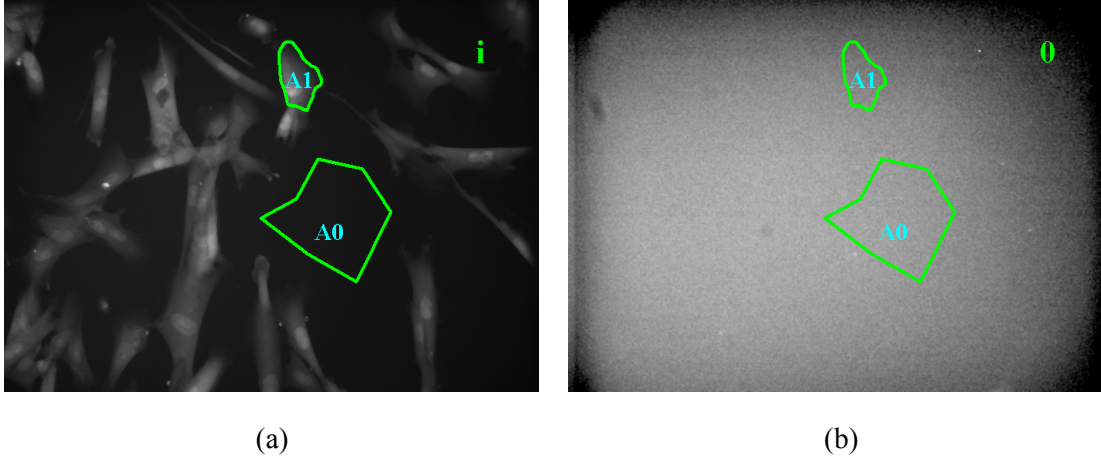


Fig. 3.9 (a): the imaging sequence of the Calcium measurement; (b): the background image taken before the imaging sequence (best-fit contrast).

Two areas **A0** and **A1** are defined in the image series (Fig. 3.9a). **A0** is free of cells and **A1** contains one cell of interest. **A0** is defined as a monitor window of the fluctuation. We assume that only the intensity of illumination fluctuates and that the illumination profile at 340 nm and 380 nm excitation keeps constant. Thus, one can evaluate the lamp fluctuation by defining the fluctuation factor  $F_i$  as:

$$F_i = \frac{\text{Brightness of area A0 in image 3.9a}}{\text{Brightness of area A0 in image 3.9b}} .$$

The whole series (at both excitations) is divided by the ratio  $F_i$ . This compensates all the images in the series to the same amount of illumination as the image Fig. 3.9b.

After the compensation, all images of the series have the same illumination level as the image Fig. 3.9b, and the compensated images should have the same fluorescence background as the image Fig. 3.9b. Therefore, one can use the image Fig. 3.9b as a background image and subtract it from the compensated image series.

Because the unevenness of illumination is different for 340 nm and 380 nm excitations and this unevenness influence the ratio of  $F_{340}/F_{380}$  in cells (for details see Section 3.3.2), one should normalize the illumination unevenness as if the whole field of view had been evenly illuminated. Assuming that the unevenness of illumination is constant at both excitations, the image series (Fig. 3.9a) should have the same unevenness of illumination as the background image (Fig. 3.9b). Therefore, one can normalize the unevenness of illumination in the compensated and background-subtracted images by dividing these images by the background image (Fig. 3.9b).

### III. Calcium Imaging System

Finally, the fluctuation-compensated, background-subtracted and normalized fluorescence images excited at 340 and 380 nm are used to create a ratio-image series of F340/F380. The mean brightness of area A1 in the ratio-image series is extracted to represent the  $[Ca^{2+}]_{cyt}$  in the cell of interest.

#### 3.4.2 the results

Fig. 3.10 shows three ways to analyze the fluorescence measurement of one experiment. The black rectangle, red circle and green triangle data represent the ratio value in a cell of interest calculated using the raw fluorescence images, the fluctuation-compensated images and the fluctuation-compensated and background-subtracted images respectively. It's evident that the compensation minimizes the noise due to fluctuation, and background subtraction increases the sensitivity of the measurement significantly. In the data shown in the sub-window of Fig. 3.10, the raw F340/F380 has a variation of 0.10 over the basic ratio of 1.0, and the  $Ca^{2+}$  peak has a maximal ratio of 1.60, which gives a signal-to-noise ratio (SNR) around 16:1; The calculated F340/F380 after the compensation and background subtraction has only a variation of 0.02, and the  $Ca^{2+}$  peak has a maximal of 1.92, which gives an enhanced SNR of 96:1.

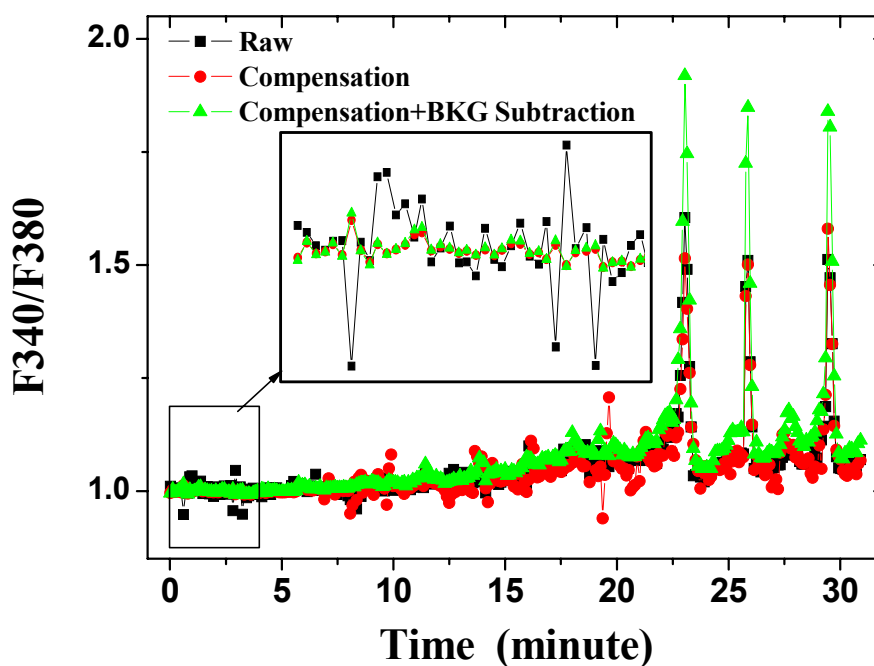


Fig. 3.10 Comparison of the calculated ratio F340/F380 after imaging processing procedures. The signal-to-noise ratio was improved after compensation and background subtraction. Black rectangles: the ratio of a cell AOI calculated using raw fluorescence images. Red circles: the ratio calculated using fluctuation-compensated images; Green triangles: the ratio calculated using fluctuation-compensated and background-subtracted images.

3.4.3 ratio image

The Calcium imaging system allows collecting a time series of 2D ratio images. However, as shown in Fig. 3.11a, the raw F340/F380 image has a bad contrast and the line histogram (Fig. 3.11c) over a cell (the pixel intensity of the green line in Fig. 3.11a) reveals no information of the cell structure at all. Background subtraction from both fluorescence images does not help to get a better contrast ratio image, because the data in Table 3.1 show that the ratio of the cellular fluorescence and that of the background fluorescence do not differ significantly from each other. In addition, even pixels in both fluorescence images have very low brightness; the ratio calculation can obtain pixels with higher brightness. For example, even when one reduce the brightness of a pixel in the background area from 110 to 5 at 340 nm excitation, and from 100 to 2 at 380 nm excitation, in the background-subtracted ratio image (F340/F380), it will give a brightness of 2.5 (instead of 1.1 as in the original ratio image).

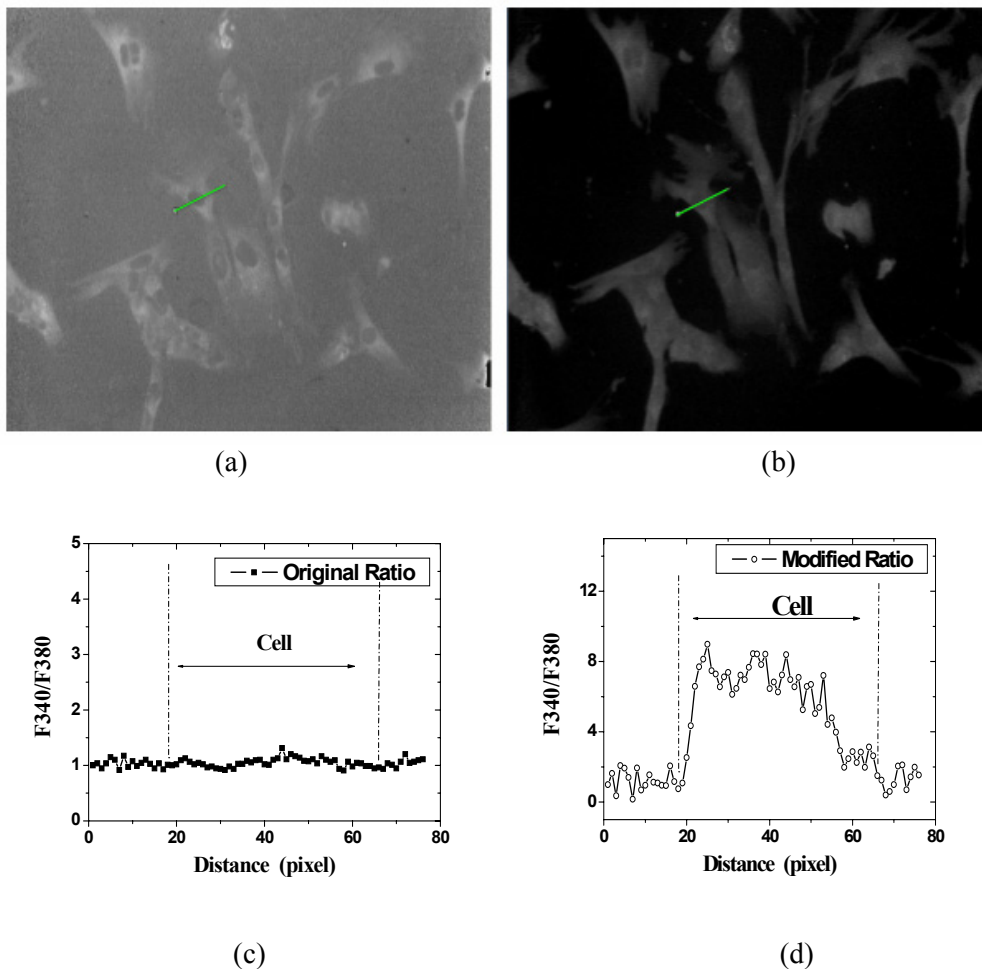


Fig. 3.11 Top: the ratio-image (F340/F380) calculated using original (a) and the background-subtracted fluorescence images (b). Bottom: the intensity histogram of the line over a cell as

### III. Calcium Imaging System

---

indicated in the top images.

A method to improve the contrast is performed on the fluorescence images. First the fluorescence images are compensated for the instability of illumination. Then the background from the F340 fluorescence images are subtracted, but the background from the F380 fluorescence images are not. The ratio image of the background-subtracted F340 images divided by the F380 images is shown in Fig. 3.11b. Clearly the ratio image calculated using background-subtracted fluorescence images gives better contrast and the line histogram reveals an enhanced ratio in the cell (Fig. 3.11d).

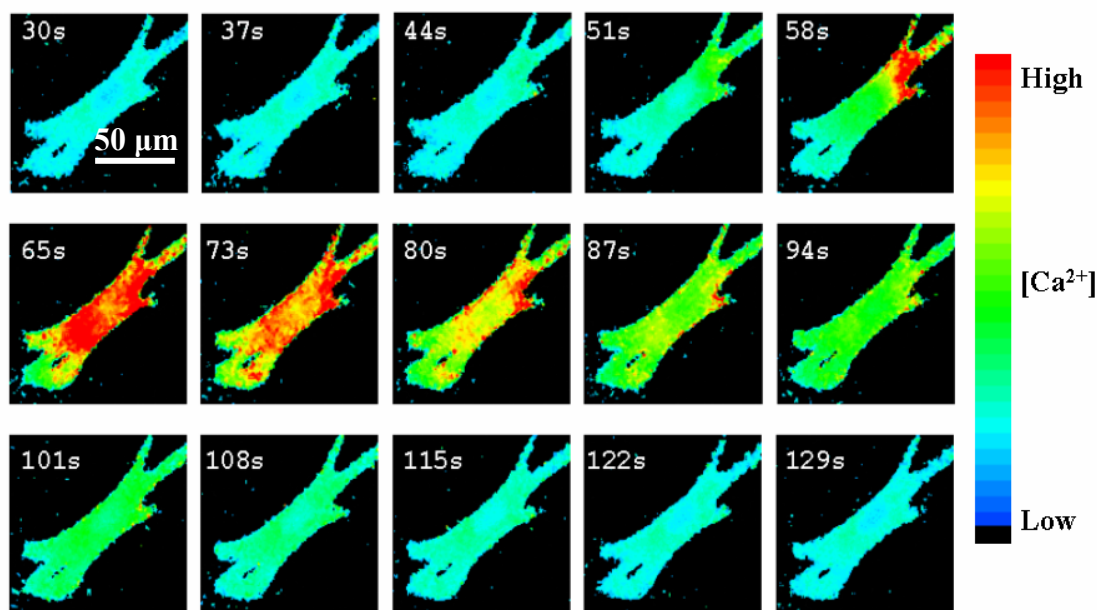


Fig. 3.12 Time series of the ratio-image shows the propagation of a  $[Ca^{2+}]_{cyt}$  wave in a AG1522-D cell (pseudo color).

Fig 3.12 shows a time series of the ratio image which reveals the propagation of a  $[Ca^{2+}]_{cyt}$  wave in a AG1522-D cell showing spontaneous Calcium oscillations. It shows that the Calcium wave started at the upper-right corner, close to the edge of the plasma membrane, propagated through the cell (including the cell nucleus), induced many Calcium sparks (red dots), and spread to the other side. This mechanism of the Calcium propagation has been reported as Calcium induced Calcium release [13]. Please see details of the spontaneous Calcium oscillation in Chapter IV.

### References

1. M. Bootman, E. Niggli, M. Berridge and P. Lipp. Imaging the hierarchical  $Ca^{2+}$  signaling system in HeLa cells. *J. Physiol.* **499**(2), 307-314 (1997).

### III. Calcium Imaging System

---

2. D.G. Todd and R.B. Mikkelsen. Ionizing radiation induces a transient increase in cytosolic free  $[Ca^{2+}]$  in human epithelial tumor cells. *Cancer Res.* **54**, 5224-5230 (1994).
3. D.W. Voehringer, M.D. Story, R.G. O'Neil and R.E. Meyn. Modulating  $Ca^{2+}$  in radiation-induced apoptosis suppresses DNA fragmentation but does not enhance clonogenic survival. *Int. J. Radiat. Biol.* **71**(3), 237-243 (1997).
4. J. Yan, K.K. Khanna and M.F. Lavin. Defective radiation signal transduction in ataxia-telangiectasia cells. *Int. J. Radiat. Biol.* **76**(8), 1025-1035 (2000).
5. S. Ringer. A further Contribution regarding the influence of the different Constituents of the Blood on the Contraction of the Heart. *J. Physiol.* **4**, 29-42 (1883).
6. E.B. Ridgway and C.C. Ashley. Calcium transients in single muscle fibers. *Biochem. Biophys. Res. Commun.* **29**(2), 229-34(1967).
7. G. Grynkiewicz, M. Poenie and R.Y. Tsien. A new generation of  $Ca^{2+}$  indicators with greatly improved fluorescence properties. *J. Biol. Chem.* **260**(6), 3440-3450 (1985).
8. A. Takahashi, P. Camacho, J.D. Lechleiter and B. Herman. Measurement of intracellular Calcium. *Physiol. Rev.* **79**(4), 1089-1125 (1999).
9. Y. Jiang and F.J. Julian. Pacing rate, halothane, and BDM affect Fura-2 reporting of  $[Ca^{2+}]_i$  in intact rat trabeculae. *Am. J. Physiol. Cell Physiol.* **273**, 2046-2056 (1997).
10. M.C. Heiß. Entwicklung und Erprobung eines Aufbaus zur gezielter Bestrahlung einzelner biologischer Zellen an der Schwerionen-Mikrosonde der GSI. Doctoral dissertation, Technical University of Darmstadt (2004).
11. W. Lohmann, C. Lohmann and M. Ibrahim. Fluorescence spectra of NADH/NAD, ynurenine, tryptophan, and tyrosine. *Naturwissenschaften* **75**(3), 141-142 (1988).
12. <http://www.usca.edu/chemistry/spectra/phenred.htm>.
13. A.P. Thomas, G.S. Bird, G. Hajnoczky, L.D. Robb-Gaspers, J.W. Jr. Putney. Spatial and temporal aspects of cellular calcium signaling. *FASEB J.* **10**(13), 1505-1517 (1996).

### Chapter IV

## The Preparatory Experiments

The aim of the Calcium imaging setup was to measure the response of  $[Ca^{2+}]_{cyl}$  to ion irradiation for a time window of 30 minutes. Because the imaging setup has no equipment to keep cells under observation in a good physiological condition, it is possible that some environmental stress might affect the measurement. It has also been reported that photo bleaching and dye leakage during fluorescence imaging influences the quantitative analysis of  $[Ca^{2+}]_{cyl}$ . In order to recognize the potential problem in the measurement performed with the ratio-imaging setup at the single ion hit facility, some preparatory experiments were performed.

### 4.1 Fura-2 Loading

The Fura-2 molecule is a hydrophilic  $Ca^{2+}$ -sensitive fluorescent dye that cannot penetrate the cellular phospholipid bi-layer membrane. Normally, the acetoxymethyl ester of Fura-2 (Fura-2/AM) is used to load Fura-2 into intact cells. The Fura-2/AM can pass the cell membrane but is not  $Ca^{2+}$ -sensitive. After the cells are loaded with Fura-2/AM, nonspecific esterases present in most cells hydrolyze the AM esters to formaldehyde and acetic acid, liberating the Fura-2 molecule [1]. Fura-2 binds to Calcium ions with a dissociation constant of around 100-300nM. It has been reported that a high concentration of Fura-2 can chelate intracellular Calcium ions, and the by-products of AM ester hydrolysis – acetate, protons and formaldehyde have potential deleterious effects on living cells [2]. Therefore, the influence of Fura-2 was examined using different concentration of Fura-2/AM in Chinese Hamster Ovary (CHO) cells.

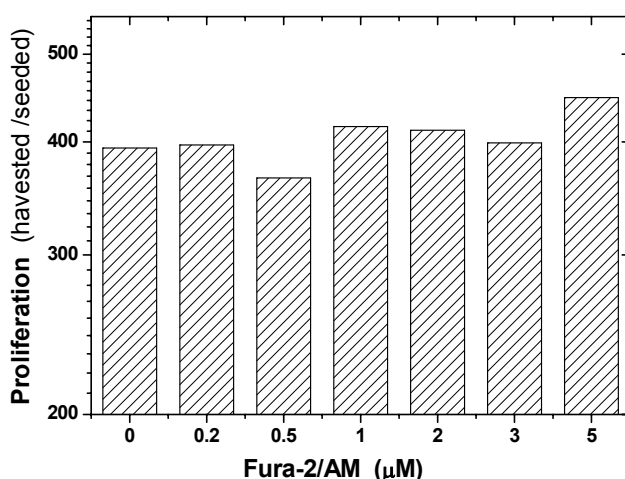


Fig. 4.1 Proliferation of CHO cells loaded with different concentrations of Fura-2/AM.

## IV. Preparatory Experiments

---

CHO cells were seeded in culture flasks with density of  $10^4/75 \text{ cm}^2$ , incubated for 24 hours ( $37^\circ\text{C}$ , 100% humidity, 5%  $\text{CO}_2$ ), then loaded with Fura-2/AM for 45 minutes at room temperature ( $\sim 22^\circ\text{C}$ , RT), rinsed 3 times and de-esterificated for 30 minutes at  $37^\circ\text{C}$  in the incubator. Some of the samples were observed using a fluorescence microscope to check the fluorescence intensity. Others were further incubated for 4 days and then harvested by trypsinization and counted using a cell counter (Z2™ COULTER COUNTER®, Beckman Coulter, Inc. USA). As shown in Fig. 3.1, no significant influence of Fura-2 on the proliferation in CHO cells was found for the loading concentration of up to  $5 \mu\text{M}$  Fura-2/AM. Finally,  $2.5 \mu\text{M}$  Fura-2/AM was chosen for the later loading protocol.

First, twenty mM HEPES medium buffer was prepared by dilution of 1M HEPES in corresponding culture medium with a final pH of 7.5. Fura-2/AM was solved in pure DMSO (Sigma-Aldrich, Germany) to prepare a 0.5 mM Fura-2/AM stock solution. Then a loading solution of  $2.5 \mu\text{M}$  Fura-2/AM was prepared by dilution of the stock solution in the 20mM HEPES buffer. In loading **protocol A**, cells were loaded in the loading solution at  $37^\circ\text{C}$  for 45 min; then rinsed three times with 20mM HEPES buffer and kept in this buffer for de-esterification at room temperature for 30 minutes. In loading **protocol B**, the cells were loaded in the loading solution at room temperature for 45 min; then rinsed three times with 20mM HEPES buffer and incubated in this buffer for de-esterification at  $37^\circ\text{C}$  for 30 minutes. Fluorescence microscopy at the imaging setup showed no significant difference of the fluorescence emission from cells stained according to these two protocols.

### 4.2 Photo Bleaching and Dye Leakage

In further experiments, the  $[\text{Ca}^{2+}]_{\text{cyl}}$  was measured in HeLa and AG1522-D cells at room temperature. As shown in Fig. 4.2 (left), the fluorescence ratio F340/F380 showed an exponential decay in 30 minutes, and the decay in cells stained using protocol A is less than that that in cells stained using protocol B.

This exponential decay of the fluorescence ratio is explained by the photo bleaching of intracellular Fura-2. Becker et al have reported that photo bleaching of Fura-2 produces an intermediate form which only fluoresces at 380 nm excitation and is not sensitive to  $\text{Ca}^{2+}$  [3]. This means even when the calcium-bound (indicated by F340) and calcium-free Fura-2 (indicated by F380) have the same bleaching constant, the effect of photo bleaching will result in a stronger loss of F340 fluorescence, producing a decay of F340/F380. In addition, because the imaging measurement was performed immediately after the de-esterification, the fact that cells loaded using protocol B (de-esterificated at  $37^\circ\text{C}$ ) showed stronger effect of photo bleaching than that using protocol A (de-esterificated at  $22^\circ\text{C}$ ) implies that fluorescein is easier to decompose under higher temperature [4]. Therefore, in further experiments, if not mentioned, all the cells were loaded with Fura-2 using loading protocol A.

## IV. Preparatory Experiments

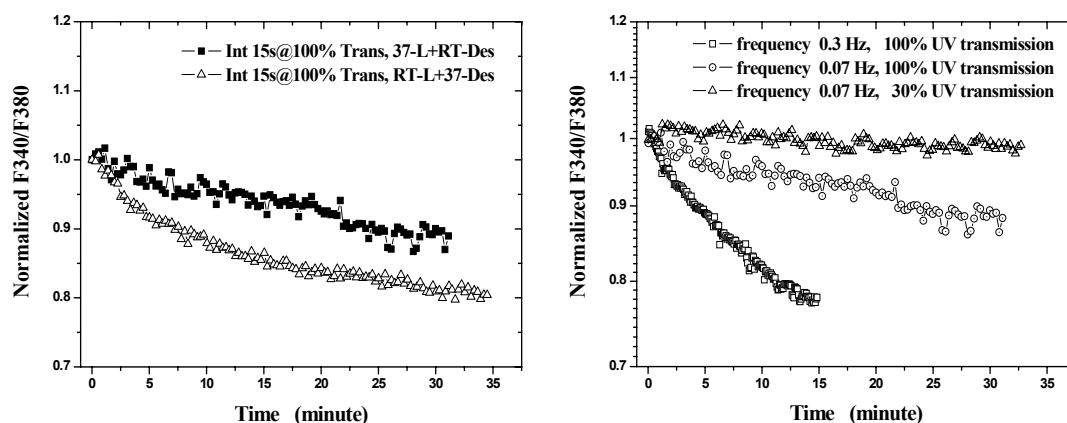


Fig. 4.2 Photo bleaching of Fura-2 in the ratiometric fluorescence imaging. **Left:** the ratio F340/F380 in HeLa cells loaded with Fura-2 using protocol A (closed rectangles) and protocol B (open triangles). The imaging was performed with UV excitation without attenuation, ratio-imaging frequency at 0.07Hz. **Right:** the ratio F340/F380 in HeLa cells using different imaging protocols (Fura-2 loading protocol A). Open rectangles: UV excitation without attenuation, ratio-imaging frequency at 0.3Hz; Open circles: UV excitation without attenuation, ratio-imaging frequency at 0.07Hz; Open triangles: UV attenuated by 30%, ratio-imaging frequency at 0.07Hz. The exposure time for both excitations was 200ms in all measurements.

The ratiometric method of Calcium measurement using Fura-2 measures the change of  $[Ca^{2+}]_{cyl}$  by the change of the fluorescence ratios (F340/F380) [1]. The decay of the fluorescence ratio will lead to a miscalculation of the  $[Ca^{2+}]_{cyl}$ . One way to reduce photo bleaching is to decrease the amount of light exposing the dye. In further experiments, the influence of photo bleaching was therefore examined in the Calcium imaging system using different imaging protocols. As shown in Fig 4.2(right), the fluorescence ratio reveals an exponential decay as a function of time with an imaging frequency of 0.3 Hz excited with 100% transmitted UV light. However, when the irradiance was 15 times less, namely with an imaging frequency of 0.07 Hz and only 30% excitation light, the fluorescence ratio kept constant rather than decreased exponentially. In other words, with the latter imaging protocol, photo bleaching has no influence on the measurement any more.

The typical decay of the fluorescence emission is shown in Fig 4.3. In resting HeLa cells, the fluorescence emission at both excitations was reduced by 20%, but the fluorescence ratio remained constant. This fluorescence decreases because the Fura-2 leaks from cytosol to the extra-cellular medium via an anion transport system [5]. In AG1522-D cells, Fura-2 leakage had no effect on the measured Calcium response based on the ratio-metric method (Fig. 4.3-right).

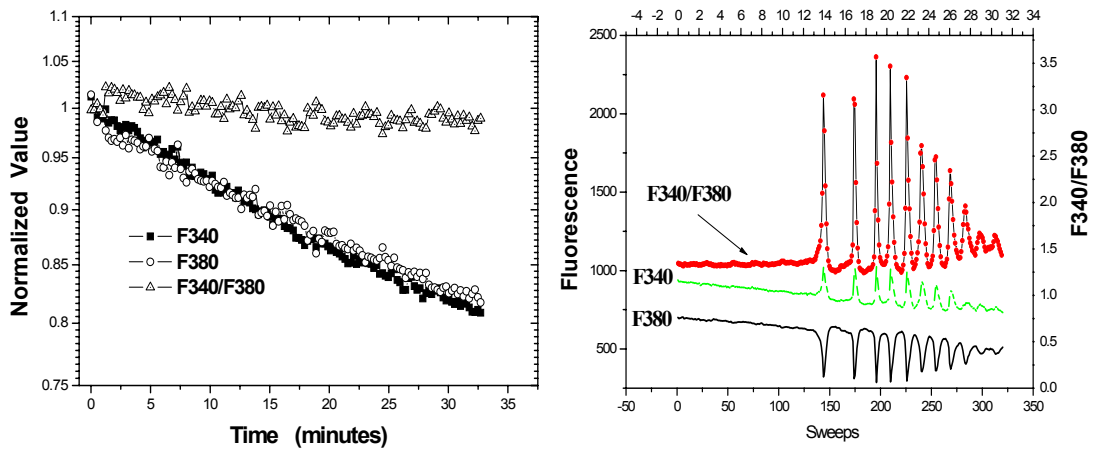
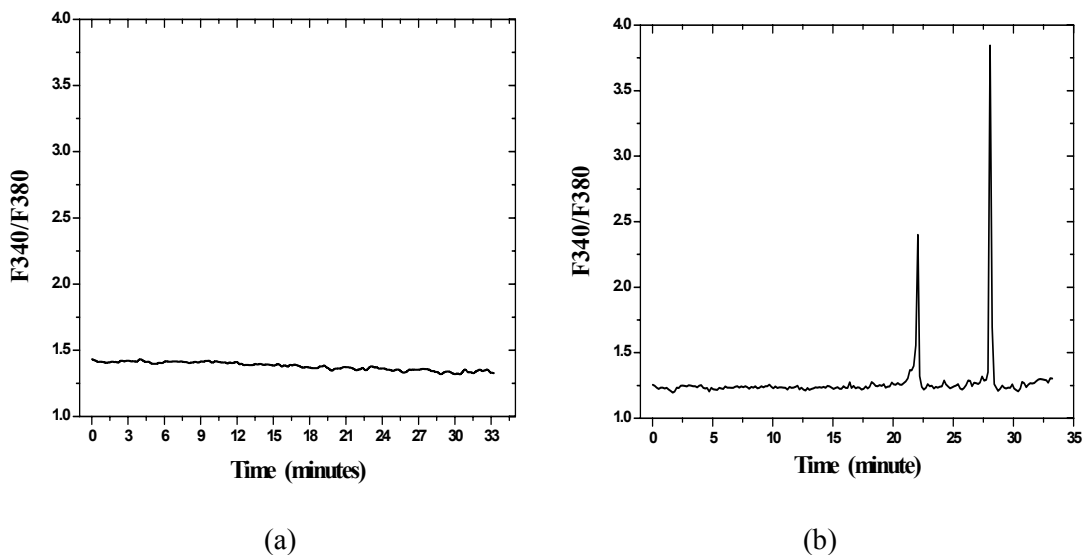


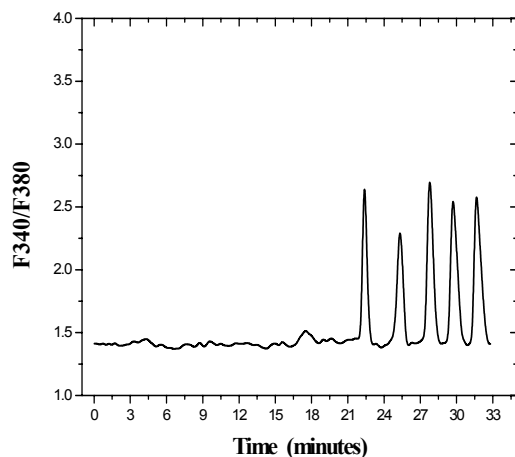
Fig 4.3 The Fura-2 leakage caused a decrease of fluorescence emission at both excitations but had no influence on the fluorescence ratio F340/F380, although the fluorescence intensity (F340 and F380) declined about 20%. Left: the ratio was constant in a resting HeLa cells. Right: the baseline ratio was constant in a responding AG1522-D cell and the dye leakage had no effect on the measured Calcium response based on the ratio-metric method.

### 4.3 Spontaneous $\text{Ca}^{2+}$ Oscillations in Fibroblasts

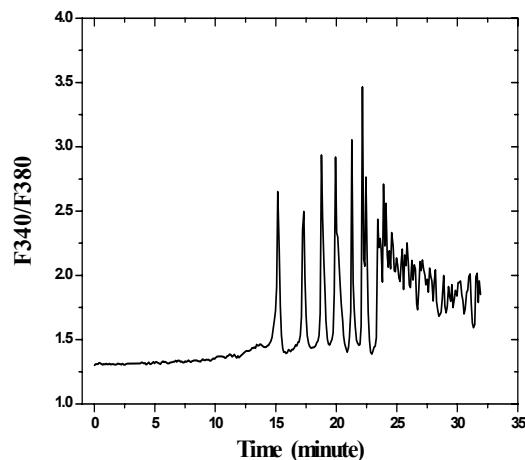
With the improved loading and imaging protocol, the intracellular Calcium in HeLa and AG1522-D cells was measured in control experiments at room temperature. It was found that the  $[\text{Ca}^{2+}]_{\text{cyt}}$  in HeLa cells is kept stable during the entire recording. In contrast AG1522-D cells revealed a complex behavior of the cytosolic Calcium



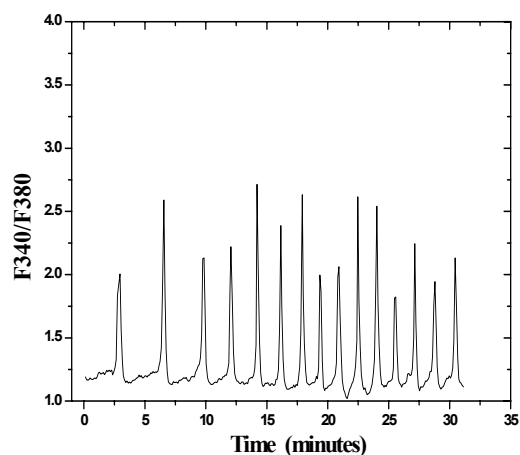
#### IV. Preparatory Experiments



(c)



(d)



(e)

Fig. 4.4 Typical  $[Ca^{2+}]_{cyt}$  behaviors in AG1522-D cells. a) constant ratio; b-d: baseline spiking starting around 20 minutes: b) spiking with long period; c) spiking with short period; d) spiking followed by an elevated rapidly fluctuating phase; e) baseline spiking starting from the beginning of the measurement.

As shown in Fig 4.4, five typical patterns of the fluorescence ratio as a function of time were found in the control experiments in fibroblast cells. Some cells kept a stable ratio (Fig. 4.4a). In many other cells  $[Ca^{2+}]_{cyt}$  revealed oscillations of different kinds: b-c) baseline spiking with short and long period, starting around 20 minutes; d) baseline spiking starting around 20 minutes followed by an elevated fluctuation; e) baseline spiking starting from the beginning of the measurement.

The mechanism underlying the baseline spiking and the elevated rapid oscillations has been reviewed in reference [6-8] and is not discussed here (see discussion in chapter V). Although one can believe that the oscillation of  $[Ca^{2+}]_{cyt}$  in the particular case of Fig. 4.4e is spontaneous [9], the oscillation in Fig. 4.4(b-c) can not be simply explained as “spontaneous oscillations” because they all start after a relative reproducible time after beginning of the experiment. The complexity of the  $[Ca^{2+}]_{cyt}$  behavior also shows that cells in the same cell dish possess different sensitivity to

some unknown stimulus. In order to find this potential stimulus, further experiments were performed.

**4.3.1 UV exposure**

At the beginning it was speculated that the stress, which induces  $[Ca^{2+}]_{cyt}$  oscillations is due to over-exposure to UV light during fluorescence imaging [10]. To test this hypothesis, the fibroblast cells were exposed to different doses of UV by using different irradiance, while keeping exposure time constant. As shown in Table 3.1, the onset of the  $Ca^{2+}$  oscillation was the same (around 20 minutes) in imaging measurements performed using different irradiance of UV excitations.

Table 3.1 Begin of  $Ca^{2+}$  oscillation in AG1522-D cells with different UV irradiances

UV irradiance* (W/m <sup>2</sup> )	Begin of $Ca^{2+}$ oscillation after (minutes)
17	19.5
34	19.5
52	20±1

\*UV irradiance were measured used a diode calibrated by an optical power meter Orion-PD

In another experiment, the Calcium imaging was performed in two fields of view at different places in the same cell dish. First, the ratio-imaging was performed at position #1 until the fibroblast cells in the field of view started to show  $Ca^{2+}$  oscillations after 20 minutes. Then, the cell stage was driven to position #2, and the ratio-imaging was continued. It was found that the fibroblast cells in the second place showed  $Ca^{2+}$  oscillations without delay. As described previously, by using an aperture in the lamp house, only the field of view was illuminated by the excitation light, which means there was no UV exposure to position #2 when the imaging was taken place at position #1 during the first 20 minutes. This shows the stress-induced  $Ca^{2+}$  oscillation is also independent from the UV exposure.

**4.3.2 temperature**

Another suspicion was that the cells were kept too long at unphysiological temperature during the measurement. Therefore, we switched on the magnet lens to warm up the cell stage to 29 °C. This generates an environment similar to the condition in the incubator (37 °C) and also simulates the environmental conditions during the beam time.

#### IV. Preparatory Experiments

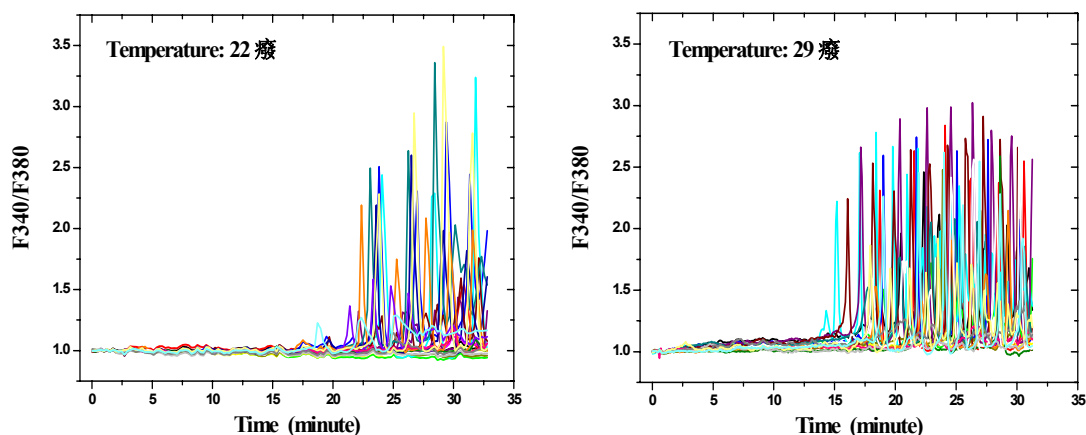


Fig. 4.5 Calcium measurement in AG1522-D cells at different temperature. Left: control experiment (22 cells) at 22 °C; Right: control experiment (22 cells) at 29 °C. The curves in the figure represent the  $\text{Ca}^{2+}$  level in different cells.

As shown in Fig. 4.5, the Calcium measurement at 29 °C, at which the temperature is closer to the physiological temperature of 37 °C did not suppress, but resulted in an even earlier onset of the  $\text{Ca}^{2+}$  oscillation and oscillations occurred in more cells (see Table 4.2). It is known that the cell metabolism is more active at physiological temperature than at a lower temperature. The fact that the oscillation appeared earlier at 29 °C than at 22 °C led us to speculate that the cellular metabolism in the closed cell dish was using up the oxygen in the medium during the measurement.

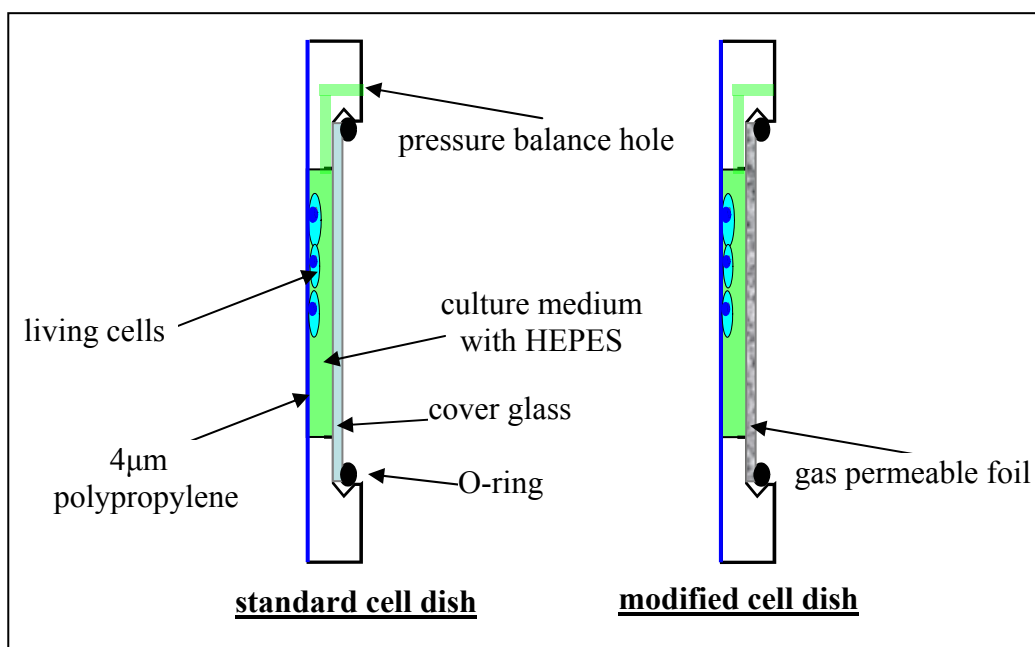


Fig. 4.6 Illustration of the cell dish used at the single ion hit facility

### 4.3.3 cell dish

A standard cell dish used for the cell irradiation at the single ion hit facility is illustrated in Fig 4.6 [11]. The cells are seeded on a Polypropylene foil pasted onto the bottom of the chamber made of stainless steel. Before the experiment, the cell dish is closed with a cover glass and vertically inserted into the cell stage as shown in Fig. 2.1. To examine the hypothesis that the lack of oxygen may have started the  $\text{Ca}^{2+}$  oscillation in AG1522-D cells, the experiment was repeated using cell dishes closed with a gas permeable foil (25  $\mu\text{m}$  thick, bioFOILIE25, In Vitro Systems & Services, Germany) instead of cover glass. As shown in Table 4.2, the population of oscillating cells was reduced to only 3% when the measurement was performed in the gas permeable cell dish, compared to 74% of oscillating cells in the standard cell dish. Hence, it is reasonable to assume that hypoxic stress caused the spontaneous Calcium oscillations in the gas-tight standard cell dish.

Table 4.2 Population of resting cells and oscillating cells in the standard and modified cell dish measured at different temperature.

Cell dish	Standard cell dish	Standard cell dish	Gas permeable cell dish
Temperature	22 °C	29 °C	29 °C
Resting cells	24 (49%)	27 (26%)	70 (97%)
Oscillating cells	25 (51%)	78 (74%)	2 (3%)

Due to technical limitations we cannot measure the oxygen concentration inside the closed cell dish. Therefore there is no proof of the decrease of oxygen concentration, but at least, it is clear that closing the cell dish with a gas permeable foil avoids the stress responsible for spontaneous Calcium oscillations. Therefore, this type of cell dish can be used to investigate the cellular Calcium response to ion irradiation at our single ion hit facility. As a byproduct of the above investigations, it may be possible to use the Calcium imaging setup for a quick test for cell stress in new designs of cell dishes.

### References:

1. G. Grynkiewicz, M. Poenie and R.Y. Tsien. A new generation of  $\text{Ca}^{2+}$  indicators with greatly improved fluorescence properties. *J. Biol. Chem.* **260**(6), 3440-3450(1985).
2. T. Tiffert, J. Garcia-Sancho and V.L. Lew. Irreversible ATP depletion caused by low concentrations of formaldehyde and of calcium-chelator esters in intact human red cells. *Biochim. Biophys. Acta* **773**, 143-156 (1984).

#### IV. Preparatory Experiments

---

3. P.L. Becker and F.S. Fay. Photo bleaching of Fura-2 and its effect on determination of Calcium concentrations. *Am. J. Physiol. Cell Physiol.* **253**, C613-C618 (1987)
4. D. Dibbern-Brunelli, M.G. de Oliveira and T.D.Z. Atvars. Temperature dependence of the photobleaching process of fluorescein in poly(vinyl alcohol). *J. Photoch. Photobio. A* **85**, 285-289 (1995).
5. P.M. McDonough and D.C. Button. Measurement of cytoplasmic calcium concentration in cell suspensions: correction for extracellular Fura-2 through use of Mn<sup>2+</sup> and probenecid. *Cell Calcium* **10**(3), 171-80 (1989).
6. A.P. Thomas, G.S. Bird, G. Hajnoczky, L.D. Robb-Gaspers, J.W. Jr. Putney. Spatial and temporal aspects of cellular calcium signaling. *FASEB J.* **10**(13), 1505-1517 (1996).
7. M.J. Berridge, Calcium Oscillations. *J. Biol. Chem.* **265**(17):9583-9586 (1990).
8. M.J. Berridge. Elementary and global aspects of calcium signaling. *J. Physiol.* **499**(2), 291-306(1997).
9. Y. Okano, T. Fu and Y. Nozawa. Calcium oscillation induced by bradykinin in polyoma middle T antigen-transformed NIH3T3 fibroblasts: evidence for dependence on protein kinase C. *Biochem Biophys Res Commun.* **176**(2), 813-819 (1991).
10. I. Ihrig, F. Schubert, B. Habel, L. Haberland and R. Glaser. The UVA light used during the fluorescence microscopy assay affects the level of intracellular calcium being measured in experiments with electric-field exposure. *Radiat. Res.* **152**(3), 303-311 (1999). E.C. Toescu, Hypoxia sensing and pathways of cytosolic Ca<sup>2+</sup> increases. *Cell Calcium* **36**(3-4), 187-199 (2004).
11. M.C. Heiß. Entwicklung und Erprobung eines Aufbaus zur gezielter Bestrahlung einzelner biologischer Zellen an der Schwerionen-Mikrosonde der GSI. Doctoral dissertation, Technical University of Darmsadt (2004).